A Demography of Galaxies in Galaxy Clusters with the Spectro-photometric Density Measurement.

Joo Heon Yoon

The Graduate School

Yonsei University

Department of Astronomy

A Demography of Galaxies in Galaxy Clusters with the Spectro-photometric Density Measurement.

A Master's Thesis
Submitted to the Department of Astronomy
and the Graduate School of Yonsei University
in partial fulfillment of the
requirements for the degree of
Master of Science

Joo Heon Yoon

December 2007

This certifies that the master's thesis of
Joo Heon Yoon is approved.

Thesis Supervisor: Sukyoung Yi

Advisor: Young-Wook Lee

Advisor: Yong-Ik Byun

The Graduate School
Yonsei University
December 2007

ACKNOWLEDGEMENTS

드디어 제 이름을 첫 페이지에 새겨진 학위논문을 마무리하게 되어서 너무나 흥분됩니다. 언제나 저의 뜻을 존중해주시고 든든한 지원자가 되어 주신 부모님, 누나, 매형에게 진심으로 감사드립니다.

벌써 3년 전 교수님께서 처음 부임하셨을 때가 생각납니다. 누구보다도 열정적인 목소리와 넘쳐나는 영감으로 학생들을 감동시킨 이석영 교수님. 교수님과의 대화를 통해 저 역시 천문학에 대한 애정을 키우고 그에 확신을 가질 수 있었습니다. 연구를 하면서 교수님의 쏟아져 나오는 수많은 새로운 아이디어와 지식들뿐만 아니라 그 순수한 열정을 배우고자 노력하였으며 앞으로도 제가 계속 공부를 해나가면서 큰 나침반이 될 것입니다. 언제나 학생들을 존중하고 배려해주셔서 감사합니다.

부심을 맡아주신 이영욱 교수님께 감사드립니다. 언제나 자신감 있는 모습을 보여주시고 연세천문학에 대한 자부심을 심어주시는 교수님. 1학년 때는 우주의 탐구를 들으며 천문학도의 꿈을 키웠고 대학원 첫 학기 때 항성진화와 종족을 들으며 스스로 생각하고 연구해 나가는 방법을 배웠습니다. 종족수업은 힘들었지만 제가 대학에서 가장 재미있게 배운 수업이었습니다.

변용익 교수님께 감사드립니다. 1학년 때 아무것도 모르고 두리번거리던 저에게 처음으로 진짜 천문학에 대해 말씀해 주셨으며 실제 연구를 하는 대학원 선배를 만날 기회를 주셨었습니다. 제가 대학에서 처음으로 교수님께 술을 얻어먹었던 게 바로 그때였습니다. 항상 핵심을 한 번에 집어내시는 교수님의 그 조언들은 제가 따라가고자 노력하는 목표가 될 것입니다.

천문석 교수님께 감사드립니다. 연세천문학의 근간을 만드시고 우리과의 가장 큰 어른이신 교수님. 교수님의 성간물질 강의를 아직도 들어보지 못한 것이 제가 아직도 해보지 못한 아쉬운 일입니다. 은퇴를 하신 후에도 계속 강의를 하

신다기에 다시 한 번 기회를 노려볼까 합니다. 항상 건강하세요.

항상 학생들에게 가장 편안하고 친근하게 대하시는 손영종 교수님께 감사드립니다. 언제나 편안하게 방으로 찾아가 대화를 나눌 수 있는 교수님이 계실 줄은 이전에는 생각도 못해봤었습니다. 수백 명의 학생들과 함께했던 교수님 우주의 이해 조교경험은 앞으로도 절대 잊지 못할 것 같습니다. 항상 학생 때의 낭만을 그대로 갖고 계신 듯 한 교수님, 교수님께서 첼로를 연주하시는 것을 보고 저도 나중에 자리를 잡으면 반드시 음악을 배우리라 결심했습니다.

항상 멘 토가 되어주신 김용철 교수님, 진지한 고민부터 사소한 일까지 언제나 찾아가면 가장 현실적이고 효율적인 답을 명쾌하게 이야기해 주셨습니다. 대학생활에서 무언가 중요한 결정을 내릴 때마다 선생님의 조언을 받지 않은 적이 없는 것 같네요. 정말 감사드립니다. 교수님께서 안식년으로 자리를 비우신 1년이 매우 길게 느껴졌습니다. 대학원 항성내부구조 수업을 꼭 들어보고 싶었는데 그럴 기회가 없어져 매우 아쉬웠습니다. 후배들을 위해서라도 꼭! 다시 부활시켜 주세요!

저와 혈육(?)이신 윤석진 교수님, 교수님께서는 언제나 놀라운 아이디어를 갖고 계신 것 같습니다. 항상 학생 스스로 찾아가도록 유도하는 교수님의 수업을 통해 힘들었지만 많은 것을 배울 수 있었습니다.

최규홍 교수님께 감사드립니다. 항상 우렁찬 목소리로 유쾌한 수업을 진행하시는 교수님, 9시 출근부를 통해 제 자신이 게을러지지 않도록 마음가짐을 다잡을 수 있었으며 항상 우리과에서 접하기 힘든 새로운 분야를 가르치셔서 새로운 세계를 알 수 있는 기회를 주셨습니다.

중후하시면서 유머감각도 뛰어나신 김석환 교수님께 감사드립니다. 중저음의 목소리로 어떻게 학문을 대하고 공부를 해나가야 하는지에 대해 해주신 말씀은 잊지 못할 것입니다. 새벽 늦게까지 추운 실험실에서 야식과 함께한 광학실험들은 가장 실질적인 수업이 아니었나 생각합니다.

박상영 교수님께 감사드립니다. 가장 많은 대학원생을 지도하시면서 학과장까지 맡으셔서 매우 바쁘실 텐데도 항상 학생들의 생활에 신경 써 주셔서 감사합니다.

같이 연구하고 토론했던 우리 GEMers!! office mate로써 1년을 함께한 이나, 우리의 노래는 끝나지 않았다. 앨범하나내자. 그나저나 그 내기는 아마 내가 이기게 될 것이다.ㅋ 최신(?) office mate 구염돌이 성희, 최근 들어 얼굴을 종종 볼 수 있어 좋네. 너네 집에 MT한번 더가자. 더불어 성희의 낭군 수영이형, 신세많이졌어요. 중얼중얼 TS 사진찍을 때 좀 웃어라. 유일한 동기 윤경이, 예전엔 GEM 끝나고 자주 한잔 했는데 요샌 뜸하다. 다시 한 번 더? 그녀가 없으면 GEM은 파산한다. 살림꾼 현진이, 쑥! Masato, as I told you before, you are the nicest Japanese who I've ever met.

7층생활 함께 했던 대학원 동기들! 모범소령님 용재형, 나만큼 유치해서 통하는 게 있는 도희, 느끼짜장크림새우깡 호선생, 페인세트 단골 인구, 적분신 로리한철, 시끄럽다 장인수, 우리과에서 제일 섹쉬한 한이, 맘씨 좋은 아침형, 반학기 함께했던 지방간 재우, 703호 보스 윤바람, 우렁찬 웃음의 원현이, 성실청년 세현이, 내밥 동윤이, 재밌었다!! 우린 다 잘 될 거야!!

우리 천문우주학과 사람들 우리 큰형님 봉봉혜원, 같이 먹은 도시락과 ㄹㅍ가 얼마더냐... 둘째 오동동신 그만 제대하여라. 요환이보다는 빨리 해야지 안그래? 징징우진 넌 결코 많이 먹는 게 아니다. 철없는 도원 중원소 부족이다. 어여 enrichment. 우리 (수)민이 대학원생은 강하게 크는 거다. 룸메서원 언제 또 같이 살지? 경석이형 곱창콜 충성할게요ㅋ. 상현아 나한테 맞는 건 괜찮은데 승천은 안 된다. 시건방 최유미 유일한 발길질 상대, 동문후배 선화 목도리 좋지? 조심재상, 호랑이 만지고 오면 인정해주마. 머라이어정화 깍듯이 모시거라. 이지혜 무한질문러쉬가 다시 시작되었구나. 묘묘 AstroNet 짱님 커피콩 먹으러 오렴. 이지롤 lala!! Twix!! 놀러와 공포영화보여줄게. 대구처녀 소희 서울사람도

친절하다규! 연구잘해보자. 재민아 영국에서 너의 요리 잊지 않으마. 문일미화 그래도 같은 버스 타는데 말 좀 잘 들어. 보스턴간 대원이형, 건담은?? 미영이 대학원 생활 잘하고, 현영이 너는 표정이 4차원일세, 호섭이 대학원 생활 잘하고, 군대있는 종현이 건강해라. 기범아 복학생의 힘! 동욱아 이제 미스리 메뉴가 다양해지겠구나, 사무조교로 고생한 성우, 매력남 용식이, 찐따 시험 준비 잘하고 현석이 군대 잘 갔다 오고, 전 회장 배현진 고생했다. 기윤, 동현, 인태, 슬희, 소진, 은송 다들 열심히 하고.

CSA에 있는 도균이형 내가 맨날 하트 보냈는데... 상일이형 여러 가지 도움 받는게 많습니다!! 남자. 철이형 멋있어요 석주형, 석주 Jr.은 언제? 후후후후... 수영아 이태원 구경좀 시켜줘라. 친절한 학섭이형, 자상한 영훈이형, 상윤아 형이 안 괴롭히니 심심하지? 혜전이 다리 빨리 회복하고, 대전으로 이사 간 창희형, 형의 내공이 그립네요 그리고 외국에 나가있는 얼굴로 승부하는 세헌이형, 쌀귀신 민수, 써라운드 난로 민영이, 많은 시간을 함께하진 못했지만 이것저것 물어보는 것에 정말 친절하게 도와준 지명국 박사님, 애리누나(놀러갈게요!!), 덕근이형, 상모형 감사합니다.

천기4반 윤호, 규보, 정진이, 동익이, 진석이, 동희, 운섭이, 정한이, 준연이, 영파, 많이도 얻어먹은 선배들 범동이형, 얼쉰형, 엄마형, 짚단형, 규승이형, 재준이형, 승준이형, 그리고 후배 원수, 웅렬이, 라동 다들 보고싶네요.

군대가기전 잊을 수 없는 추억과 학점을 남긴 연세대 최고 밴드 가이아!!. 윤찬이형, 유석이형, 형준이형, 종혁이형, 한민이형, 덕중이형, 재희형, 태오형, 호준이형, 영록이형, 용택이형, 상배형, 요한이, 주현이, 성언이, 성욱이, 승민이, 정두, 석준이, 영훈이, 인재, 마수, 상래, 윤석이, 태우, 세영이 이하. 고등학교를 함께 했던 상민이, 형훈이, 창규, 찬도, 동식이, 상길이, 윤호, 빠리, 관형이 술 한 잔 하자!!

Kevin who is my co-author, I have found hotter food than the fire-chicken.

Martin, shall we have North Korean beer again? Ignacio, Thanks a lot for your help!!

많이 부족하지만 쏟은 열정만큼 자부심을 갖고 있는 논문입니다. 모두가 있었기에 이렇게 완성할 수 있었습니다. 다시 한 번 감사드립니다.

Contents

List of Figures

List of Tables

ABSTRACT

Galaxy clusters are the densest regions in the Universe and useful laboratories for testing galaxy evolution theories. We study the environmental dependence of galaxy properties in galaxy clusters. In order to study that, we need a well-defined catalog of galaxy clusters and their member candidates. Galaxy redshift surveys, such as the Sloan Digital Sky Survey, provide 3-d information that makes it possible to construct a homogeneous and unbiased catalog. However, the spectroscopic survey is hampered by the incompleteness problem mainly due to the fiber collisions. This problem makes it difficult to find overdense regions and to measure realistic local densities of galaxies. Therefore, we try to minimize the incompleteness problem by using the color-magnitude relation (CMR). With the new method added on the spectroscopic selection of neighboring galaxies, we measure a spectro-photometric density of galaxies and construct galaxy cluster catalog with 924 clusters of which 212 are new. We study how the luminosity and color of galaxies vary with clustocentric radius. The median magnitude and color of galaxies hardly show clustocentric dependence. The fractions of early-type galaxies and red galaxies decrease with the clustocentric radius whereas late-type and blue galaxies show the opposite trend. The tendency could come from the morphology-density relation. This radial dependence gets stronger for denser clusters implying that the environment has something to do with the morphology of galaxies. We also investigate the nature of the brightest-cluster galaxies (BCGs). The BCG luminosity depends on the local density while colors do not. The density dependence of BCG luminosity reveals little difference with that of the 2nd or 3rd BCGs. The different photometric properties of BCGs

referred by many authors seem to be spawned not by their innate nature but by their environment. We also study the environmental effect on cluster and non-cluster galaxies and find that the non-cluster galaxies are bluer than cluster galaxies for a fixed magnitude.

Key words : catalogs — surveys — galaxies: clusters: general

Chapter 1

Introduction

Galaxy clusters are the most dense regions in the large-scale universe. The number density of galaxies in clusters can be several hundred times larger than that of the field. They are thus ideal laboratories for studying the effect of environment on the formation and evolution of galaxies.

The first galaxy cluster catalogs (Abell, 1958; Zwicky et al., 1961-1968; Abell, Corwin, & Olowin, 1989) were based on the visual inspection of photographic plates. While these catalogs have been widely adopted, they suffer from many selection effects and spurious detections due to projection effects. Furthermore, the visual inspection of large parts of the sky is very time consuming. Systematic searchers for galaxy clusters are needed to ensure the efficiency and reliability of the cluster detection. Among the most popular in the absence of spectroscopic information were the technique using the early-type galaxy color-magnitude relation (Gladders & Yee, 2000) and finding brightest cluster galaxies (Bahcall et al. 2003; von der Linden et al. 2007). The first automatic search for optical clusters looking for overdense regions was by Shectman (1985) followed by numerous

others (Lumsden et al., 1992; Dalton et al., 1994; Postman et al., 1996; Croft et al., 1997; Kim et al., 2002; Kochanek et al., 2003; Miller et al., 2005).

With the advent of large-area, spectroscopic redshift surveys, such as the SDSS and 2dF surveys (York et al., 2000; Colless et al., 2001; Stoughton et al., 2002), large cosmological volumes with redshift have become available. We are finally able to systematically search for galaxy clusters in a large volume by measuring the local 3-d number density of galaxies. While the 3-d densities measured based on the spectroscopic database are more powerful than projection-based 2-d searches for delineating the local galaxy distribution, they require a high level of coverage of member galaxies in the spectroscopic survey a priori. However, even the most up-to-date surveys (such as the SDSS) show only $\sim$ 60–70% completeness rate in dense regions, hampering us from measuring the densities accurately. In this thesis, we introduce an improved method for finding galaxy clusters by measuring local densities using both *spectroscopic* and *photometric* data, and provide a new catalog of the clusters we have found.

The role of environment in the formation and evolution of galaxies is a topic of much interest in modern astrophysics. Dressler (1980) found that the abundance of early-type galaxies increases in dense environment indicating that environment has an effect on galaxy morphology. This *morphology-density relation* has been further studied by many authors (e.g., Whitmore & Gilmore, 1991; Dressler et al., 1997; Goto et al., 2003; Capak et al., 2007; Park et al., 2007) and has been extended to lower density regions and high-redshift clusters (Postman & Geller, 1984; Giovanelli, Haynes, & Chincarini, 1986; Tully, 1988). There have been several physical mechanisms proposed to explain this relation, such as ram pressure stripping (Gunn & Gott, 1972; Farouki & Shapiro, 1980; Fujita & Nagashima,

1999; Abadi, Moore, & Bower, 1999; Quilis, Moore, & Bower, 2000; Chung et al., 2007), tidal forces (Byrd & Valtonen, 1990; Valluri, 1993), galaxy harassment (Moore et al., 1996, 1999), starvation (Larson, Tinsley, & Caldwell, 1980), and interaction and merging (Toomre & Toomre, 1972; Makino & Hut, 1997; Bekki, 1999; Boselli & Gavazzi, 2006; Chung et al., 2007).

Some of these processes involve violent gas dynamics, and hence it is quite likely that environment influences the star formation rate in galaxies (Gisler, 1978; Larson & Tinsley, 1978; Lewis et al., 2002; Gomez et al., 2003; Christlein & Zabludoff, 2005; Elbaz et al., 2007). The cosmic star formation history itself is also suspected to depend on environment (Thomas, Maraston, & Bender, 2005). Perhaps as hints of these suspicions, galaxy properties such as color, luminosity, and size appear to depend on environment (Balogh et al., 2004a,b; Blanton et al., 2005; Croton et al., 2005; Postman et al., 2005; Quintero et al., 2006; Park et al., 2007). However, the exact physical processes that link between galaxy properties and environment are still far from being clear. Hence, we try to unravel the environmental effect on galaxies residing in the clusters with our catalog.

Brightest cluster galaxies show different features compared with other bright elliptical galaxies. BCGs have the distinct photometric characters (von der Linden et al., 2007; Liu et al., 2007) and some of them may still have star formation features (Quillen et al., 2007). The different properties could be caused by the distinct formation history. The several formation mechanisms of BCGs such as galactic cannibalism (Ostriker & Tremaine, 1975; White, 1976; Ostriker & Hausman, 1977), tidal stripping (Gallagher & Ostriker, 1972; Richstone, 1975; Merritt, 1985), and the star formation by cooling flows (Silk, 1976; Fabian, 1994)

are proposed. The suggested mechanisms are mostly related to the environment where brightest cluster galaxies reside. With our catalog including the new density measurement, we try to explain the different photometric properties which could help us understand the formation and evolution history of central galaxies.

We assume cosmological parameters $\Omega_m = 0.3, \Omega_\Lambda = 0.7, q_0 = -0.55$, and $H_0 = 70$ km s^{-1} Mpc^{-1} throughout this thesis, and all distances are comoving.

Chapter 2

The Data

The SDSS is performing a survey to cover a quarter of the whole sky. The imaging survey of the SDSS DR5 contains 215 million objects in 8000 deg^2. The SDSS spectroscopic survey mapped 5740 deg^2 obtaining about a million spectra of which 674,749 objects are classified as galaxies. The galaxy redshifts provided make it possible to study 3-d structure of galaxy distribution.

The SDSS photometric pipeline provides several kinds of magnitudes. For galaxy colors, we use the `modelMags` as they provide unbiased colors regardless of any color gradients. For galaxy luminosities, we use `petroMags` as these are a better estimate of the total luminosity (Stoughton et al., 2002). We also apply a K-correction as described in Blanton et al. (2003b) and correct for Galactic extinction with the Schlegel, Finkbeiner, & Davis (1998) values provided by the SDSS pipeline.

We use the SDSS DR5 both photometric and spectroscopic data. For the galaxies with spectra, we extract *all types of galaxies* in the range $0.05 < z < 0.1$ and having $r_{\rm petro} < 17.77$ (Strauss et al., 2002). At $z = 0.1$, $r = 17.77$

corresponds to an absolute magnitude of $M_r = -20.55$. In order to create a volume-limited sample and so avoid biases with redshift, we cut at this absolute magnitude.

For galaxies without spectra, we select all galaxies with $13.00 < r_{\rm petro} < 17.77$ to have the same apparent magnitude cut as the spectroscopic data. Its faint limit comes from the SDSS spectroscopic survey limit, and the bright limit is from the fact that the objects of $r_{\rm petro} < 13.00$ and $z > 0.05$ are almost always stars rather than galaxies.

Chapter 3

Measuring Galaxy Density [1]

3.1 Local Density Measurement

Popular methods to measure galaxy local densities include a simple estimation of spatial number density in a certain radius and the distance to the nth nearest galaxy (Gomez et al., 2003; Balogh et al., 2004a; Miller et al., 2005; Capak et al., 2007). The number density, however, cannot tell us about the concentration status which is critical for studying dynamical evolution, while using the nth nearest galaxy can be biased by local density fluctuations. Thus, in addition to the number density, the spatial separation between galaxies can be taken into account as well to provide additional information. For example, closer neighbors can be weighted more than distant galaxies. Schawinski et al. (2006) (hereafter S06) introduced such a weighting scheme with a Gaussian filter. The

[1] Yoon, Schawinski, Sheen, Ree, & Yi, 2008 ApJS in press (astro-ph/0712.1054)

S06 scheme considers neighboring galaxies in the ellipsoid defined by:

$$\left(\frac{r_a}{3\sigma}\right)^2 + \left(\frac{r_z}{3c_z\sigma}\right)^2 \leq 1, \tag{3.1}$$

where σ is the searching distance criterion, r_a is the projected distance and r_z is the line-of-sight distance, all in Mpc, to a neighboring galaxy. It allows all the galaxies within the ellipsoid to be counted for measuring the density. The c_z factor is a simple compensation for "the finger-of-god" effect due to the peculiar motion and is estimated by counting the number of galaxies n within the sphere of radius σ as:

$$c_z = 1 + 0.2n \tag{3.2}$$

where n is capped at 10. Hence, this can scale along the radial direction up to a factor of 3. Density measures by adopting a fixed volume in comoving space can lead to sample vastly different volumes in the field and in clusters due to the stretching of the line of sight direction by the finger-of-god effect.

The density parameter to each member galaxy based on the spectroscopic data is calculated as

$$\rho_{\mathrm{spec,3D}}(\sigma) = \frac{1}{\sqrt{2\pi}\sigma} \sum_i \exp\left[-\frac{1}{2}\left(\frac{r_{a,i}^2}{\sigma^2} + \frac{r_{z,i}^2}{c_z^2\sigma^2}\right)\right] \tag{3.3}$$

by summing up for all the members within the search ellipsoid. The target galaxy is not included in the density summation. Our algorithm estimates the local density with surrounding galaxies in a relatively large area and thus minimizes local effects.

In this thesis, we attempt to improve the density measurement scheme of S06 by adding photometric member candidates and build on the S06 algorithm to design an effective cluster search method.

3.2 Member Selection with Spectroscopic Data

Since we do not have the line-of-sight information on the photometric member galaxies, we first measure the 2-d densities for our spectroscopic galaxy samples ignoring the line-of-sight information.

We first define an ellipsoid as in S06:

$$(\frac{r_a}{\sigma_1})^2 + (\frac{r_z}{\sigma_2})^2 \leq 1. \tag{3.4}$$

We choose $\sigma_1 = 1\,\mathrm{Mpc}$ because it optimizes the search for the density peak and the brightest cluster galaxy of the cluster. For σ_2 we adopt the distance corresponding to three times the velocity dispersion of the cluster. Note that σ_2 is used only for selecting member galaxies but not for the 2-D density measurement. Readers are referred to §3.5 for more details. Galaxies within the ellipsoid are regarded as member galaxies of the cluster. Then the new 2-d density ρ_{spec} for the spectroscopic members is:

$$\rho_{\mathrm{spec}} = \frac{1}{\sqrt{2\pi}\sigma_1} \sum_i \exp\left[-\frac{1}{2}\left(\frac{r_{a,i}^2}{\sigma_1^2}\right)\right] \tag{3.5}$$

where $\sigma_1 = 1\,\mathrm{Mpc}$.

3.3 Member Selection with Photometric Data

The SDSS spectroscopic survey tries to cover galaxies as complete as possible with a tiling algorithm (Blanton et al., 2003a). However, its selection scheme can leave some galaxies unobserved due to fiber collisions. Figure 3.1 shows the extreme case of Abell 2670 which shows only 65% of spectroscopic coverage rate within the 1 Mpc radius from the cluster center. This effect is generally worse for denser regions because the fiber collision problem is obviously worse in the more crowded regions. We estimate the spectroscopic completeness, that is, the number fraction of galaxies covered by the SDSS DR5 spectroscopic survey, to be $f_{\rm spec} \sim 65\%$ for rich clusters. An independent study has also reported that 30% of true brightest cluster galaxies are missed by the spectroscopic survey (von der Linden et al., 2007). The "incompleteness" of the spectroscopic survey causes a problem in measuring the densities of galaxies in dense regions. We attempt to alleviate this by further considering photometric data.

Early-type galaxies in clusters have a tight correlation between their optical colors and luminosity, known as the color-magnitude relation (CMR). The CMR was first observed by Baum (1959) and is often reported to be universal within errors (Visvanathan & Sandage, 1977; Hogg et al., 2004; López-Cruz, Barkhouse, & Yee, 2004). Based on these assumptions, we can select candidate cluster members even though they do not have redshift because galaxies on the CMR have a high likelihood of belonging to the cluster. Thus, we find the slope and scatter of the CMR in order to select "photometric members". For small clusters, the slope of the CMR can be difficult to achieve. Hence, we construct an empirical CMR by stacking galaxies that are members of 20 typical clusters determined by their redshifts. We do this for five redshift bins with $\Delta z = 0.01$,

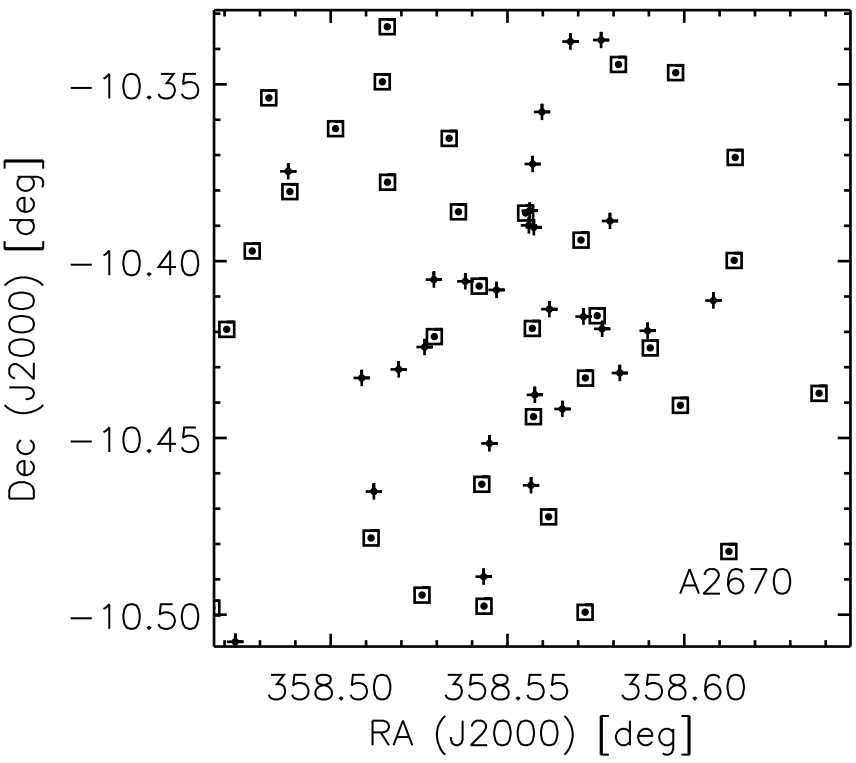

Figure 3.1: The spectroscopic completeness for the case of Abell 2670 with $r_{\rm petro} < 17.77$. The dots with rectangles are galaxies covered by the SDSS spectroscopic survey and the crosses are the missed ones. The completeness rate for this cluster is only 55% in this field of view and 65% within 1 Mpc radius from the cluster center. This figure illustrates the problem of fiber collisions in dense environments.

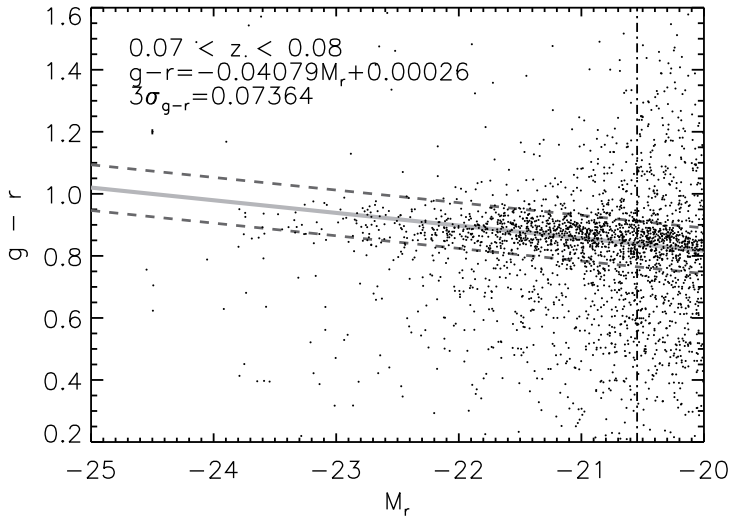

Figure 3.2: Empirical CMR for the redshift range $0.07 < z < 0.08$. The gray-solid line shows a linear fit after 2σ clipping until the number of galaxies on the CMR becomes constant and the dashed lines show the scatter (the gray-solid line $\pm 3\sigma$ in $g - r$ color). The vertical dot-dashed line is a absolute magnitude cut in our data selection.

and an example is shown in Figure 3.2. A linear fit with $2\,\sigma$ clipping is iterated until the number of galaxies on the CMR remains constant. The galaxies residing on the CMR $\pm(3 \times rms)$ in $g - r$ color are selected as "photometric members". We compute the 2-d photometric density $\rho_{\rm phot}$ following Eq. 3.5 using only the photometric members.

The total density ρ of a galaxy is calculated by combining the spectroscopic

and photometric density parameters:

$$\rho = \rho_{\rm spec} + \rho_{\rm phot}. \tag{3.6}$$

In the process of combining $\rho_{\rm spec}$ and $\rho_{\rm phot}$ we are losing the line-of-sight information and our density measures are projected into only two dimensions; but, our method still provides improved density measures as will be demonstrated in Chapter 4. through our follow-up spectroscopic observations.

When we determine whether a particular galaxy without redshift belongs to a cluster as described in this section, we assume that the galaxy is at the redshift of the cluster and apply the same absolute magnitude cut as discussed in §2.

We have attempted improving our local density measure further by applying a galaxy luminosity weight (i.e. weighting more luminous galaxies more) but found no significant difference. Hence, we have decided to ignore it.

3.4 The Efficiency of the CMR technique

We expect that the CMR to be effective for finding cluster member galaxies but that it may still suffer from the projection effect of background and foreground objects. Hence, we test its efficiency. We restrict the test on the spectroscopic data only, because only with redshift we can determine whether a particular galaxy is a cluster member or not, that is, for a convincingly high confidence. Besides, we use early-type galaxies alone for this test as our CMR method works only for them. In order to select early-type galaxies (ETGs), we use the morphological index *fracDev* from the SDSS pipeline, which shows the weight of the de Vaucouleurs profile in the two-component profile fit with the de

Vaucouleurs and exponential profiles. We apply the highly conservative r-band $fracDev > 0.95$ cut, and the galaxies selected are highly likely to be early type. Using the spectroscopic members meeting the same $fracDev$ criterion, we check the validity of our scheme defining the following two CMR-related quantities.

$$\text{Completeness} = \frac{\text{\# of ETG members in CMR}}{\text{\# of all ETG cluster members}} \times 100 \tag{3.7}$$

$$\text{Purity} = \frac{\text{\# of ETG members in CMR}}{\text{\# of ETG galaxies in CMR}} \times 100 \tag{3.8}$$

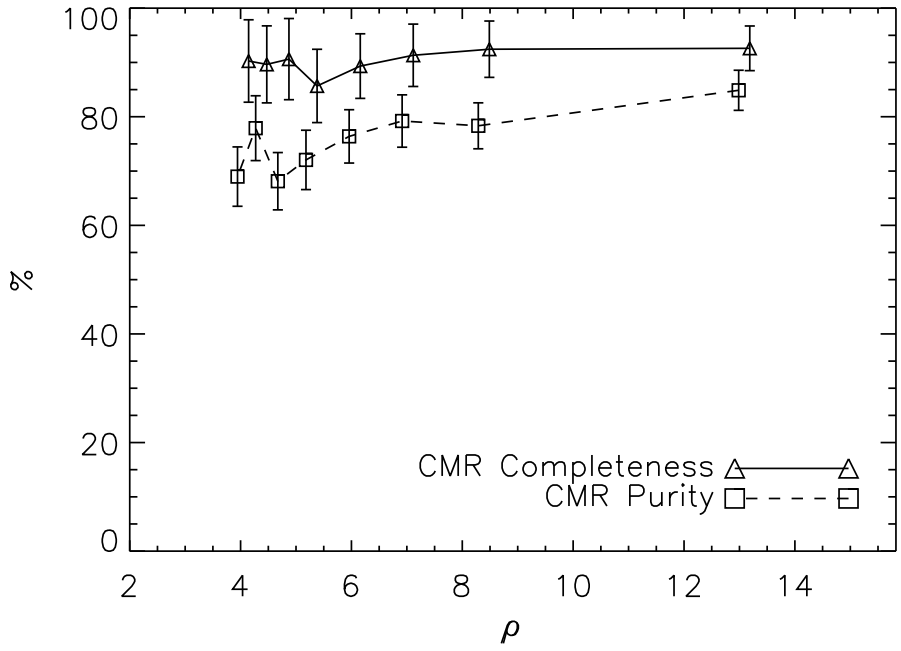

Figure 3.3: The solid and dashed lines show completeness and purity of the photometric member candidates found from our technique (see the text for definition). The errors are from the Poisson statistics in the equal number bin. The rectangles are shifted slightly to the left for the clarity of the figure. The completeness is constantly $\sim 90\%$ and the purity is 70–85% with an apparent density dependence. The high values of these parameters validate our CMR technique.

The "CMR completeness" is a measure of the number of the early-type cluster members that also sit on the CMR. The "CMR purity" tells us the fraction of galaxies selected by the CMR method that are indeed early-type cluster members. Figure 3.3 presents the CMR completeness and purity of our clusters as a function of density. The CMR completeness is around 90% meaning that 90% of the early-type (by $fracDev$) member galaxies indeed sit on the CMR. The purity is 70–85% meaning that only 70–85% of the galaxies on the CMR are early-type (by $fracDev$) members. The rest may be background or foreground galaxies. Exact values of these parameters modestly depend on the $fracDev$ criterion adopted, but on the whole both parameters show high values validating our scheme.

3.5 Finding Clusters

The SDSS DR5 photometric data includes about a million galaxies in the magnitude range described in §2. Searching for clusters through the entire data set would require an exhaustive amount of effort. So we begin our cluster search first by estimating the local density of *spectroscopic* members and identify about 7000 galaxies with high density measures as candidate cluster positions. For this selection we use 3-D spectroscopic density parameter ($\rho_{\rm spec,3D} > 0.5$).

We then select all the photometric and spectroscopic galaxies within a 2 Mpc radius from the cluster center candidate galaxies and estimate their total 2-d local density with both the spectroscopic and photometric members for all galaxies in this radius.

With these 2-d spectro-photometric density measurements, we find the galaxy with the highest density in the area of a 2 Mpc circle and $\Delta z = 0.01$. The highest

density galaxy in a local area is defined as the maximum-density galaxy (hereafter MDG). As the MDG resides at the densest part of the selected volume, we define it as the cluster center and declare it a cluster if the ρ of an MDG is greater than 4.0 which roughly corresponds to a cluster velocity dispersion of $200\,\mathrm{km\,s^{-1}}$.

We *expect* that the MDG should be close to the cluster center and coincide with the brightest cluster galaxy (BCG; Matthews, Morgan, & Schmidt 1964; Oegerle & Hill 2001). We compared the projected separation of BCGs to MDGs and found that they do not always coincide, however. We assume that a good cluster search scheme should identify MDGs as BCGs as well, and thus we vary the member search radius (the short axis of the ellipsoid) hoping to minimize the separation.

Figure 3.4 shows the separation between MDGs and BCGs. The mean and error bars reflect the large scatter in the sample. The median is a better estimate of the typical distance and shows a convergence towards a lower value of search radius. But too small a value of the search radius would miss too many member galaxies in the density measurement and be dominated by local density fluctuations. The typical virial radius of our clusters is 0.5 Mpc in the 2-d projection, and a substantial fraction ($\sim 50\%$) of clusters have a virial radius greater than 0.5 Mpc and extends beyond 1 Mpc. Considering this, we have chosen 1 Mpc as our search radius. It should be noted that our search using spectroscopic data and the CMR is liable to missing clusters that are dominated by blue, star-forming galaxies, if any.

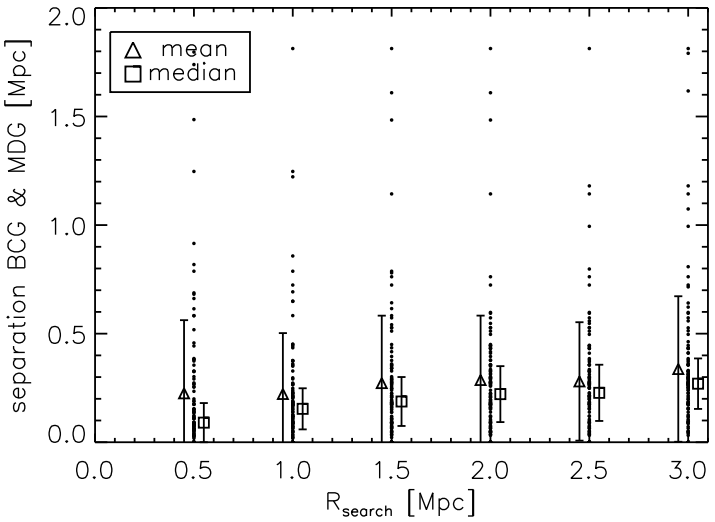

Figure 3.4: The projected separation between brightest cluster galaxies (BCGs) and maximum-density galaxies (MDGs). Triangles are the mean and squares are the median separations. The error bars show the standard deviation for the mean and the median absolute deviation for the median. When the search radius to find member galaxies is 1 Mpc, the separation is small enough that the cluster search is effective. But a substantially smaller values than 1 Mpc would miss many member galaxies because the typical size of clusters can be easily as large as 1 Mpc (see the text).

Chapter 4

Cluster Catalog [1]

4.1 Cluster Catalog and Properties

We provide our cluster catalog in Table 4.1. We have found 924 galaxy cluster candidates with $\rho \geq 4.0$ which roughly corresponds to $200\,\mathrm{km\,s^{-1}}$. Among them, 212 clusters are newly found in this study.

Table 4.1 provides various properties of our galaxy clusters. The positions of MDGs and BCGs are included. The redshift of each cluster is obtained by finding the redshift peak of the spectroscopic members and fitting it by Gaussian function. When the number of spectroscopic members is less than 4, we simply find median redshift of spectroscopic member galaxies. We calculate the virial radius r_{200} by counting the number density of member galaxies and comparing it to the cosmological background number density of galaxies. We estimate the number of galaxies within a virial radius N_{200} by counting the galaxies within r_{200}. The velocity dispersion is calculated with biweight estimator (Beers, Flynn, & Gebhardt, 1990) in r_{200} after 3-sigma clipping. As a proxy to the cluster size

[1] Yoon, Schawinski, Sheen, Ree, & Yi, 2008 ApJS in press (astro-ph/0712.1054)

and density, we can use ρ regardless of the cluster size (virial radius).

Figure 4.1 shows a sample from the newly-found clusters. The BCG and MDG are marked as number 1 and 7, respectively. Blue and red circles denote photometric and spectroscopic members, while the size of circles is proportional to the galaxy r-band brightness. Postage images of the member galaxies are also shown. Its MDG is ranked 142th out of 924, with $\rho = 9.1$ and $N_{\rm gal} = 16$ within 1 Mpc. For comparison, the central galaxy in the Virgo cluster, M87, has $\rho = 7.5$ and $N_{\rm gal} = 19$ within 1 Mpc, and thus is comparable.

Table 4.1: Cluster catalog with $\rho \geq 4$

(1)	(2)	(3)	(4)	(5)	(6)	(7)	(8)	(9)	(10)	(11)	(12)
ID	ra_{MDG} (J2000)	dec_{MDG} (J2000)	z_{clt}	ρ	N_{200}	R_{200} [Mpc]	σ_v [$km\,s^{-1}$]	ra_{BCG} (J2000)	dec_{BCG} (J2000)	z_{BCG}	Comments
1	258.20851	64.05295	0.08257	32.197	148	2.785	1299	258.12006	64.06076	0.07340	A2255
2	358.55746	-10.39042	0.07623	29.234	91	1.842	840	358.55703	-10.41904	0.07766	A2670
3	208.26551	5.13824	0.07945	25.020	50	1.421	780	208.27667	5.14974	0.07890	A1809
4	228.81884	4.37958	0.09796	24.611	65	1.487	864	228.80879	4.38621	0.00000	A2048
5	255.66908	33.52032	0.08819	22.783	74	1.813	1135	255.63809	33.51666	0.08640	A2245
6	239.58334	27.23342	0.08969	22.476	190	2.918	1000	239.58334	27.23342	0.09081	A2142
7	205.54886	2.22449	0.07688	21.140	41	1.286	845	205.54018	2.22721	0.00000	A1773
8	186.91015	8.82133	0.08981	20.599	41	1.305	849	186.87809	8.82456	0.00000	A1541
9	230.33576	30.67093	0.07845	19.313	76	1.723	677	230.33576	30.67093	0.07845	A2061
10	255.64172	34.07809	0.09871	19.178	64	1.546	1120	255.67708	34.06003	0.09891	A2244

Column 1: ID; Column 2,3: the coordinates of the maximum-density galaxies (MDGs); Column 4: the redshift of clusters estimated with spectroscopic data; Column 5: the density of the cluster MDG within 1 Mpc; Column 6: the number of member galaxies of clusters within R_{200}; Column 7: the virial radius of clusters obtained by the number density profile of the galaxy clusters; Column 8: the velocity dispersion within R_{200}; Column 9,10: the coordinates of the brightest-cluster galaxies (BCGs); Column 11: the redshift of the BCGs. The entries with zero mean the absence of the redshift information; Column 12: matching result with known catalog of galaxy clusters. The complete version of the galaxy clusters is available on the web-page http://gem.yonsei.ac.kr/Yonsei_galaxycluster_catalog.txt.

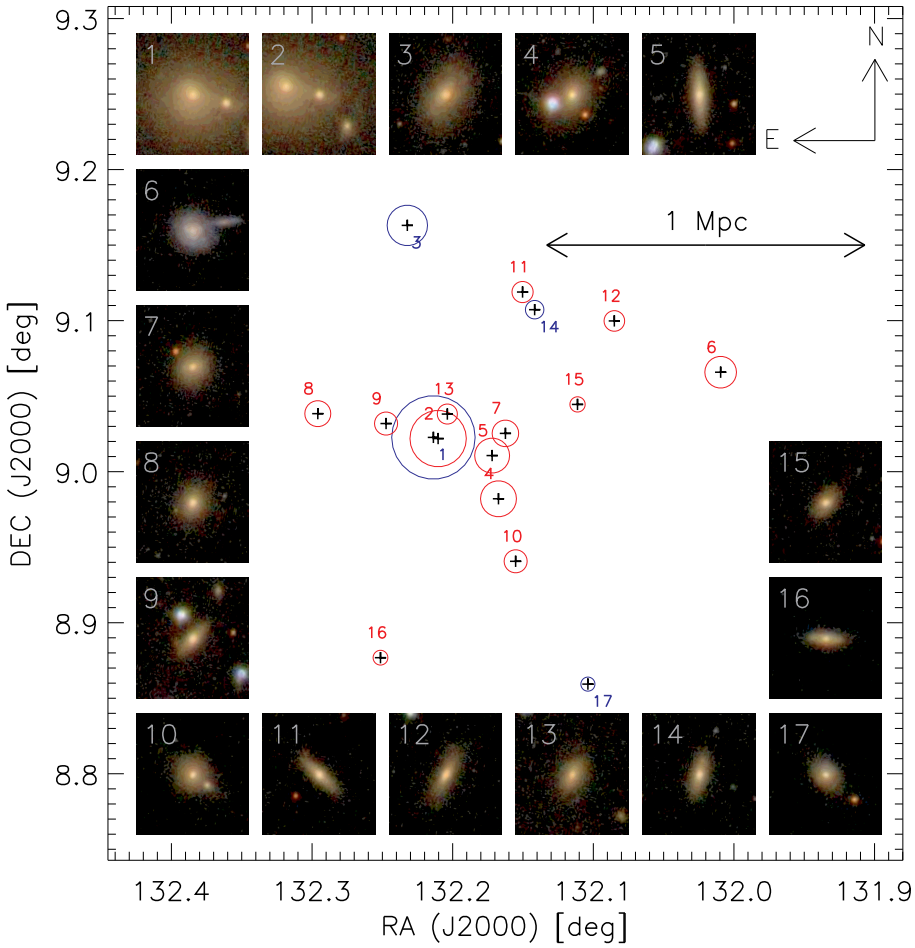

Figure 4.1: A sample rich cluster that is newly found in our study. The density ranking is 142th, out of 924, with the density parameter $\rho = 9.1$ and $N_{\rm gal} = 16$ within 1 Mpc, where its virial radius R_{200} is estimated to be 0.737 Mpc and $N_{200} = 11$. The size of each circle denotes its r-band luminosity. Blue and red circles show photometric and spectroscopic members, respectively. SDSS image cut-outs are shown for the 16 members and the central MDG (number 7). The BCG is marked as number 1.

In §3.5, we introduced the separation between the MDGs and BCGs as a test of how well the cluster search scheme finds cluster centers. In Figure 4.2, we show the separation between MDGs and BCGs in our method with (bottom) and without (top) added photometric members. It illustrates the effectiveness of the added photometric members.

The galaxy number density profile is a good proxy for the mass profile and thus dark matter profile of galaxy clusters (Carlberg et al., 1997; van der Marel et al., 2000; Katgert, Biviano, & Mazure, 2004; Lin, Mohr, & Stanford, 2004; Hansen et al., 2005). In Figure 4.3, we show the galaxy number density profile of two examples. We compare them with the Navarro-Frenk-White (NFW) dark matter profile (Navarro, Frenk, & White, 1996), which is defined as

$$\frac{\rho(r)}{\rho_c} = \frac{\delta_c}{(r/r_s)(1+r/r_s)^2}, \tag{4.1}$$

and can be projected into a 2-dimensional space as

$$\frac{\rho(r_p)}{\rho_c} = 2n_0 \int_0^{\theta} \frac{\delta_c}{(r_p/r_s cos\theta)(1+r_p/r_s cos\theta)^2} d\theta \tag{4.2}$$

where n_0 is normalization factor, r_p is projected distance and $\theta = cos^{-1}\frac{r_p}{r_{200}}$. The number density profile is in reasonable agreement with the NFW profile as found also by Hansen et al. (2005). The galaxy number density profile only based on the spectroscopic members is lower than the one with photometric members added. The departure gets larger in the central region of the clusters where the spectroscopic coverage is poor.

A larger cluster would have a higher value of ρ, the density measure within 1 Mpc. We show the distribution of ρ, N_{200} and the velocity dispersion of clusters

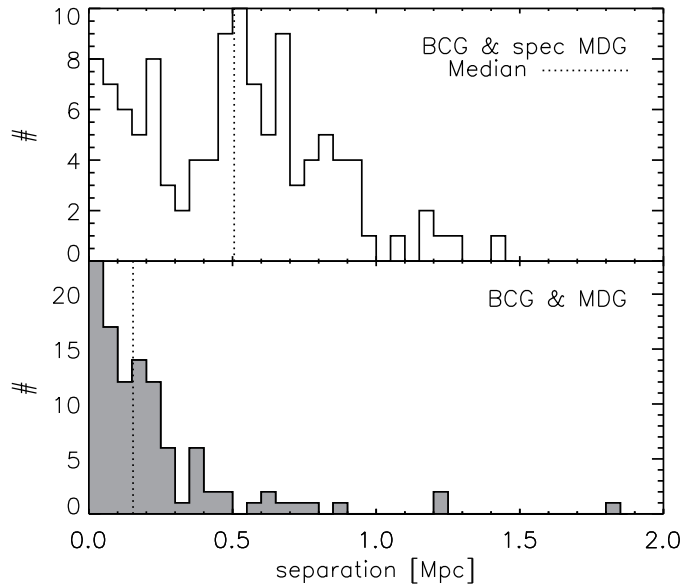

Figure 4.2: We show the separation between BCGs and MDGs. The dotted lines represent the median separation. The top panel shows the separation when the CMR-selected photometric members are not included in the density measurement. When we add the photometric members (bottom), the separation gets much smaller yielding a more reliable cluster center detection.

within r_{200} in Figure 4.4. The (minimum, median, and maximum) for the four panels are (0, 5, 190) for N_{200}, (4.0, 5.7, 32.2) for ρ, (0, 263, 1299) for σ, and the redshift range is 0.05 through 0.1.

The density and the velocity dispersion of M87 (Binggeli, Tammann & Sandage, 1987) in Virgo cluster is shown as well.

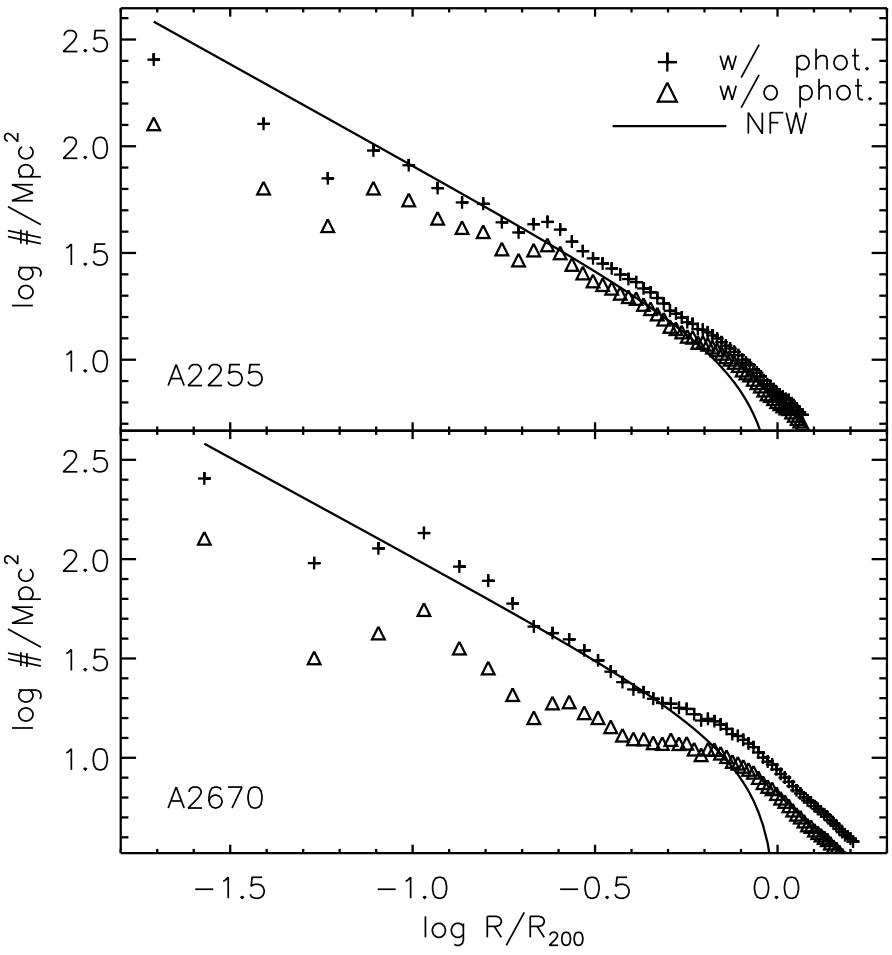

Figure 4.3: The projected radial profiles of the galaxy number density of sample rich clusters centered at their BCGs. The plus signs show the galaxy number density profiles from our scheme (including both spectroscopic and photometric members), and the triangles are those with only spectroscopic members. Also shown for comparison are the projected NFW halo profiles fitted to our measurements *with* both spectroscopic and photometric members. Our measurements are in good agreement with the projected NFW profiles.

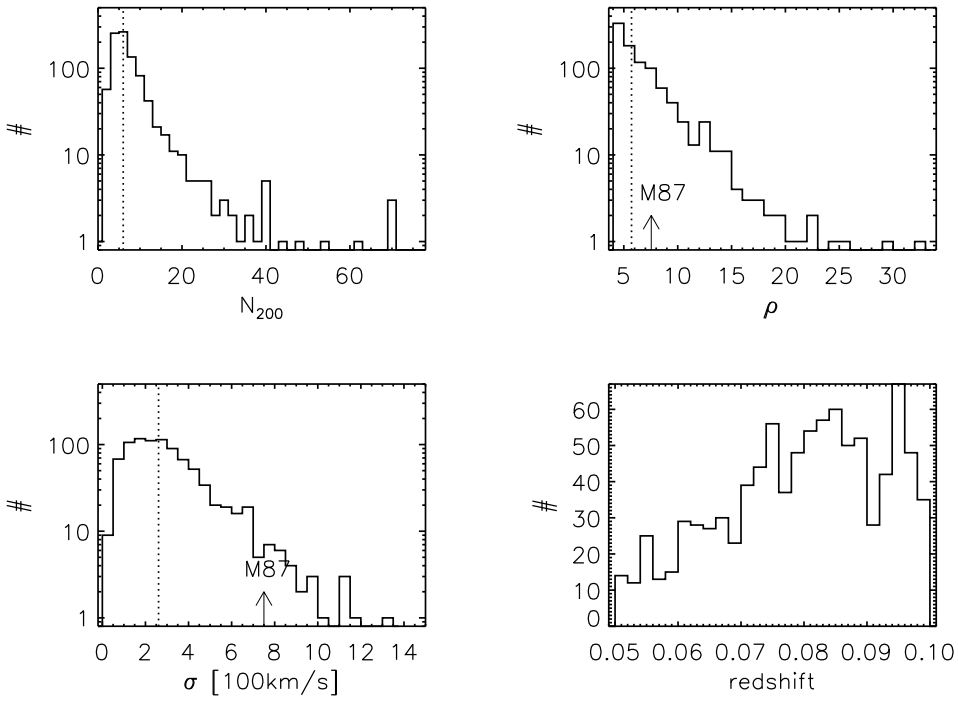

Figure 4.4: Histogram of N_{200}, ρ, velocity dispersion, and redshift. We define galaxy clusters when a condition $\rho \geq 4.0$ is met. In the top left panel two clusters of $N_{200} = 190$ and 148 are out of bound. The vertical dotted lines show median values. The density and velocity dispersion of M87 are shown as the arrow.

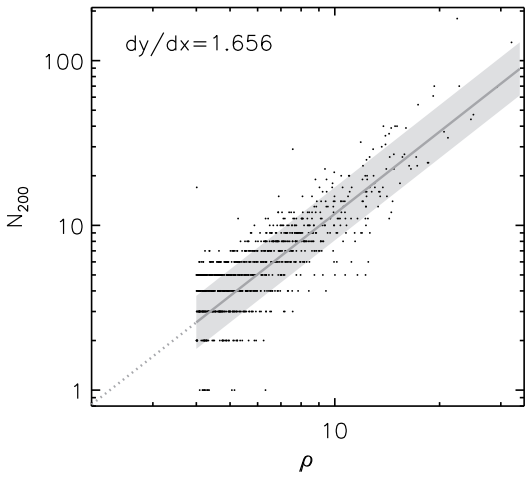

Figure 4.5: The density parameter ρ is proportional to N_{200} scaling as power law. Note that the density parameter includes the distance information in addition to the number. The thick line is the linear fit to the data and the grey band shows the standard error of the fit.

In Figure 4.5 we compare ρ with N_{200}. Also shown is the linear fit to the data. The density parameter ρ appears to scale as a power law with N_{200} rather than with a linear relation. That is, in dense regions, the linear fit would have a steeper slope. This is because the Gaussian weight in our density measuring scheme takes the distance to each member into account. For a given number of cluster members, a more concentrated cluster would have a higher value of ρ.

In Figure 4.6 we compare between various cluster properties. The density parameter is a good proxy to the size of galaxy clusters. It also shows a good correlation with the velocity dispersion of clusters. Thus, our density parameter can be an obvious indicator of dynamical mass of a galaxy cluster as well.

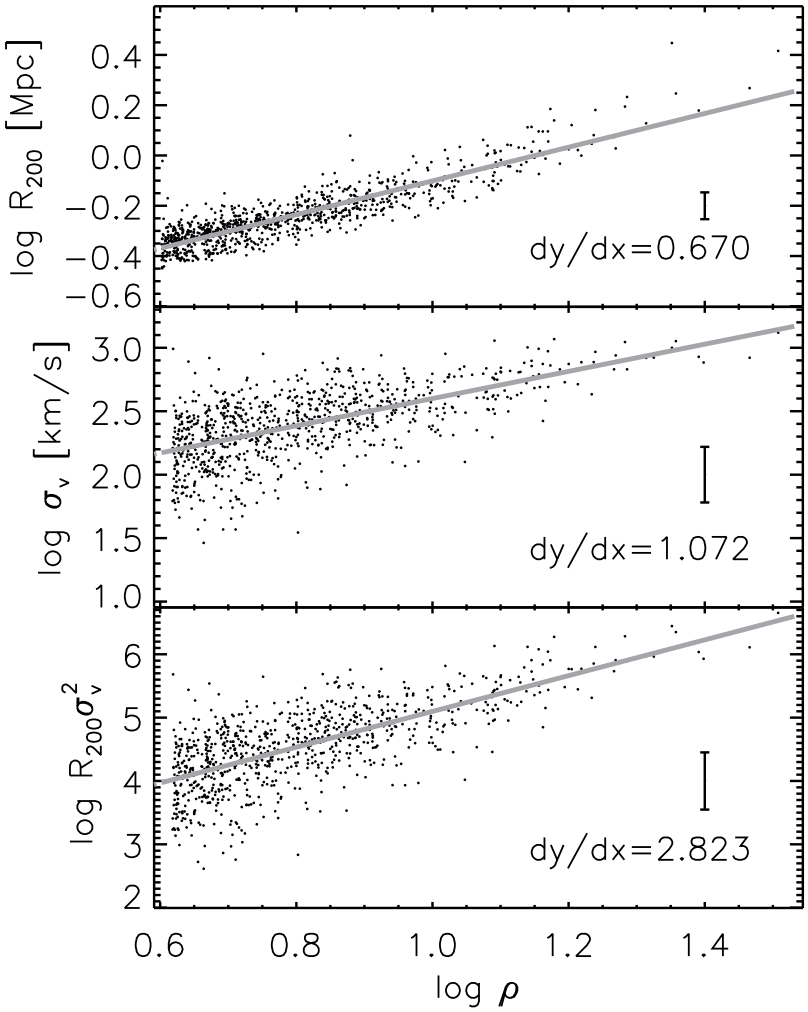

Figure 4.6: The density parameter ρ is in agreement with the properties representing the mass and size of clusters. The virial radius in the top panels has a tight correlation with ρ. The density parameter correlates with the velocity dispersion and dynamical mass in the middle and bottom panels. The thick gray line is our linear fit and dy/dx presents the exponents of the power law. The error bars represent mean scatter.

4.2 Comparison to other catalog

We perform a cross-matching between existing catalogs and ours. The matching criteria are 2 Mpc in the projected radius and $\Delta z = 0.01$. When the known clusters do not have redshift (e.g., Zwicky clusters), we just match them within 2 Mpc radius in the sky. Each cluster in our catalog is matched with other catalogues separately. The clusters that are detected in our method are generally in the existing catalogs (See Table 4.2). Most of rich clusters are matched with Abell or Zwicky clusters and this implies that the new algorithm using MDGs successfully finds rich galaxy clusters. For those clusters in the existing catalogs which include redshift, we can check the rate at which our method recovers clusters known previously. Some Abell clusters have redshifts and the C4 catalog clusters always do (Miller et al., 2005). We cross-check our clusters against the Abell and C4 clusters that are in the SDSS area and in our redshift range. 128 out of 162 Abell clusters with redshifts and 300 out of 458 C4 clusters are detected in our method, corresponding to detection rates of 79% and 66%, respectively. When we lower the ρ cut for "clusters" from 4.0 to 1.0 we would find 89% and 95% of Abell and C4 clusters, respectively. For example, by using a $\rho = 1$ cut, we can recover additional 18 Abell clusters. However, such a low value of cut ($\rho \sim 1.0$) would also find significantly more cluster candidates (3,959) many of which may be false detection. Our density measures with $\rho = 4$ cut are in general based on about 7 member galaxies. Besides, when only a small number of galaxies are used for density measurement, the density measures become less reliable, too. Since our goal is to construct a database of galaxy clusters with *improved* and hence reliable density measures, we think our $\rho = 4.0$ cut is a good compromise. However, we admit that this choice is still somewhat arbitrary and

Table 4.2: The number of galaxy clusters found in our scheme matched to previous catalogs.

Cluster Catalog	Number	Recovery(%)
Abell	128	79%
Zwicky	457	
C4	300	66%
Others	889	
Newly Found	212	
Total	924	

Note — The existing cluster catalogs are from the VizieR Catalog Service.

having this cut we are neglecting smaller clusters. In this regard, our 924 cluster candidates represent a robust sample of relatively-rich clusters.

The galaxy clusters that were known to Abell but missed by our method are mostly due to the ρ cut as mentioned above. In addition, our method missed 9 Abell clusters which are mainly composed of relatively faint galaxies that do not make it to our volume-limited sample. Two Abell clusters were missed because they are found by our method to be parts of larger clusters, just like the M87 and M49 groups in Virgo cluster. Five additional clusters were missed due to various minor reasons: e.g., mismatch in the redshift of the center galaxy of a cluster, mismatch in the position of the center galaxy of a cluster, and so on.

We compare our new catalog to the C4 cluster catalogue (Miller et al., 2005). While we use the density ρ to represent the richness of a cluster, the C4 Catalogue provides the number of galaxies within various radii. We compare our density measures within 1 Mpc, ρ, with the C4 richness (C4 parameter wmag1000) in

Figure 4.7. The match is reasonably good but shows a large scatter. The systematic difference in vertical scale has a couple of critical origins. Most importantly, our limiting magnitude, $M_{\rm r} = -20.5$, is somewhat brighter than that of C4 (-19.9). Secondly, our density is not a simple count of galaxies but weighted by the distance from the cluster center. Thirdly, our method, unlike C4, includes additional photometric member candidates. Fourthly, our choice for the search radius (1 Mpc) is smaller than that of C4 ($1/h$ Mpc). Lastly, the member-search volume in C4 is a cylinder with a line-of-sight length corresponding to four times the velocity dispersion, while ours is an ellipsoid with a length that is 3 times the velocity dispersion. The large scatter is mainly a result of two effects. To begin with, the position of the central galaxy of a cluster can be different mainly because our method includes photometric member candidates. In addition, the redshift of a cluster can also be different. We notice some difference in the velocity dispersion measured as well, which also contributes to the scatter.

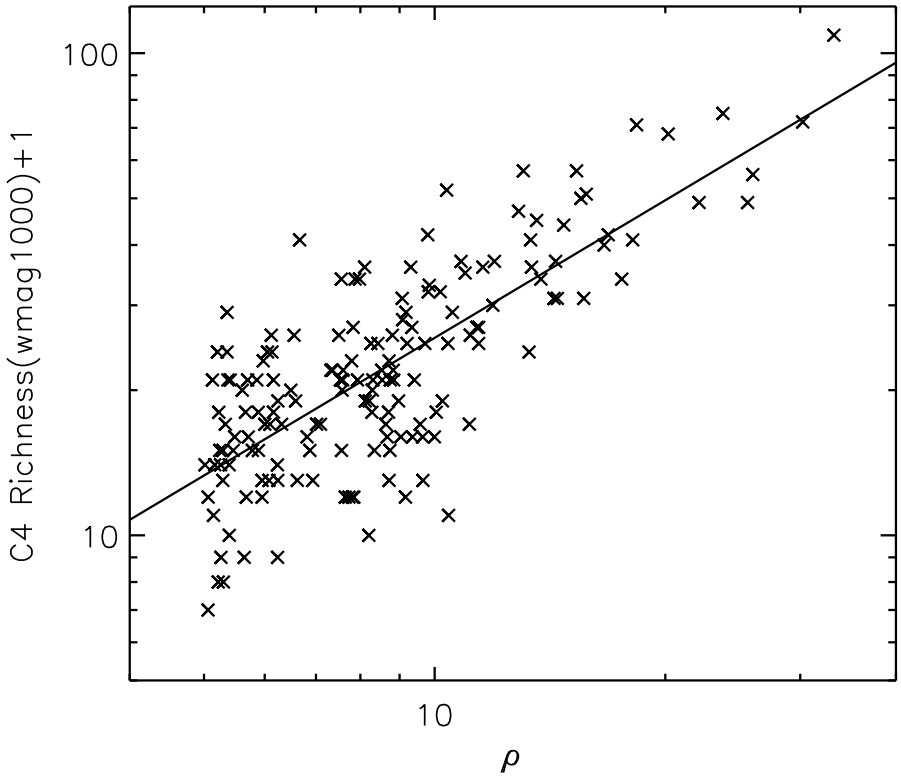

Figure 4.7: Comparison between catalogs in terms of the richness of the clusters. X-axis shows our density parameter ρ (listed in Table 4.1) and y-axis shows $N_{\rm gal}$ (wmag 1000) from the C4 catalog. The large scatter has several origins (see text for details). The line shows the linear fit.

4.3 Effects of photometric members

The inclusion of the CMR-selected photometric members increases our local density measures by $\sim 22\%$ (See Figure 4.8). In this figure, the small black dots show the density measures of our clusters based only on the SDSS database. A linear fit to the data is shown as a dashed line (showing the 22% increase) and the one-to-one relation is presented as a dotted line.

To check the validity of the CMR technique further, we attempt to recover our spectro-photometric density *approximately* by dividing the measured spectroscopic density $\rho_{\rm spec}$ by the estimated spectroscopic completeness fraction $f_{\rm spec}$. Figure 4.9 compares $\rho_{\rm spec}/f_{\rm spec}$ (crosses) with our spectro-photometric density ρ (the upper ends of arrows). They agree reasonably well. Since ρ is a complex parameter including the distance information while $f_{\rm spec}$ is not, we also make the comparison to $N_{\rm gal}$, which also shows a tight correspondence.

4.4 Additional spectroscopy for the test

For 22 of our clusters we were able to find 2dF spectroscopic data with which we identified further member galaxies. Using these new spectroscopic members, we computed new (enhanced) $\rho_{\rm spec}$ and compared them to our SDSS-spectro-photometric ρ in Figure 4.9. The x axis shows our 2-d SDSS-spectroscopic density ($\rho_{\rm spec}$) that suffers from the incompleteness problem. The y axis shows density measures improved upon $\rho_{\rm spec}$ through various methods. The blue filled circles show the new spectroscopic density measures for the 22 clusters including the added 2dF member candidates: $\rho_{\rm spec,SDSS+2dF}$. Only a few of the new SDSS+2dF spectroscopic density measures ($\rho_{\rm spec,SDSS+2dF}$) overshoot our

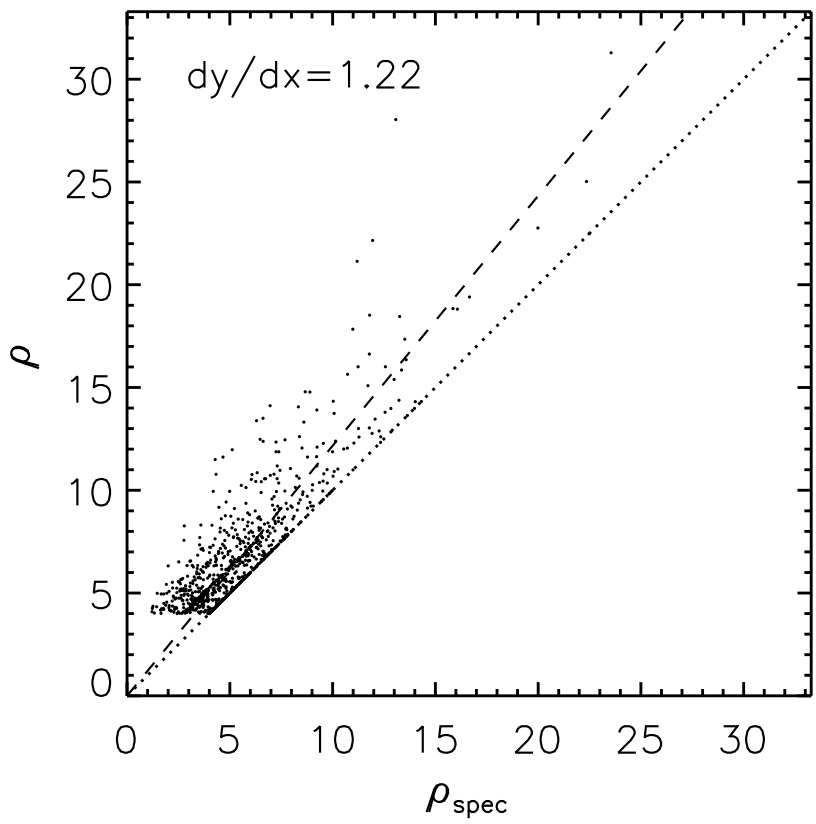

Figure 4.8: We compare our density measure ρ with $\rho_{\rm spec}$ (the density only with spectroscopic data). The dotted line presents the one-to-one relation between ρ and $\rho_{\rm spec}$ and the dashed line shows a linear fit with the y-intercept fixed at the origin. The departure gets larger in dense regions. The density increases by 22% through the addition of photometric member galaxies.

22% enhancement prediction (dashed line). Even in this case, however, the SDSS+2dF spectroscopic density measures ($\rho_{\rm spec,SDSS+2dF}$) are still lower than our SDSS-only spectro-photometric density measures ($\rho_{\rm spec+phot,SDSS}$; that is, our density measures in Eq. (3.6) in most cases, as indicated by the arrows. The end points of the arrows indicate our SDSS-spectro-photometric density measures.

In order to test our result, we have performed CTIO Hydra MOS observation of Abell 2670 and significantly increased the spectroscopic coverage of this cluster from 65% (within 1 Mpc) to 92%. We chose this cluster as a test case because it suffers from an extreme case of the spectroscopic incompleteness problem as mentioned in §3.3.

The observation was performed on 1–3 December 2006 with Hydra, a Multi-Object-Spectrograph mounted on Blanco 4m-Telescope at CTIO. The wavelength range covers 3600–8000Å and the spectral resolution is 2.3Å/pixel with mean signal-to noise ratio of 13. The target selection was totally independent of SDSS data. All of the early-type galaxies in Abell 2670 with $r < 18$ were mainly selected as targets but we also tried to cover late-type galaxies as many as possible, too. In order to execute our plan as completely as possible, we used three fiber-configurations to evade fiber collision issues in dense regions. For each fiber configuration, a total of 45 minutes which consists of 3 exposures of 15 minutes was taken for median combine and cosmic-ray removal. All the processes are done mainly with IRAF `hydra` package. The radial velocities of galaxies were measured by cross-correlation method using IRAF `rvsao` package and cross-correlation templates of SDSS. In the top right of Figure 4.9, we show our new SDSS+CTIO spectroscopic density ($\rho_{\rm spec,SDSS+CTIO}$) at ≈ 25 (purple

diamond at the top right). The value, based on a relatively complete (92%) spectroscopic survey, now is a factor of two larger than the previous $\rho_{\rm spec,SDSS}$ and much closer to our spectro-photometric density $\rho_{\rm spec+phot,SDSS}$. This validates our spectro-photometric density measurement scheme.

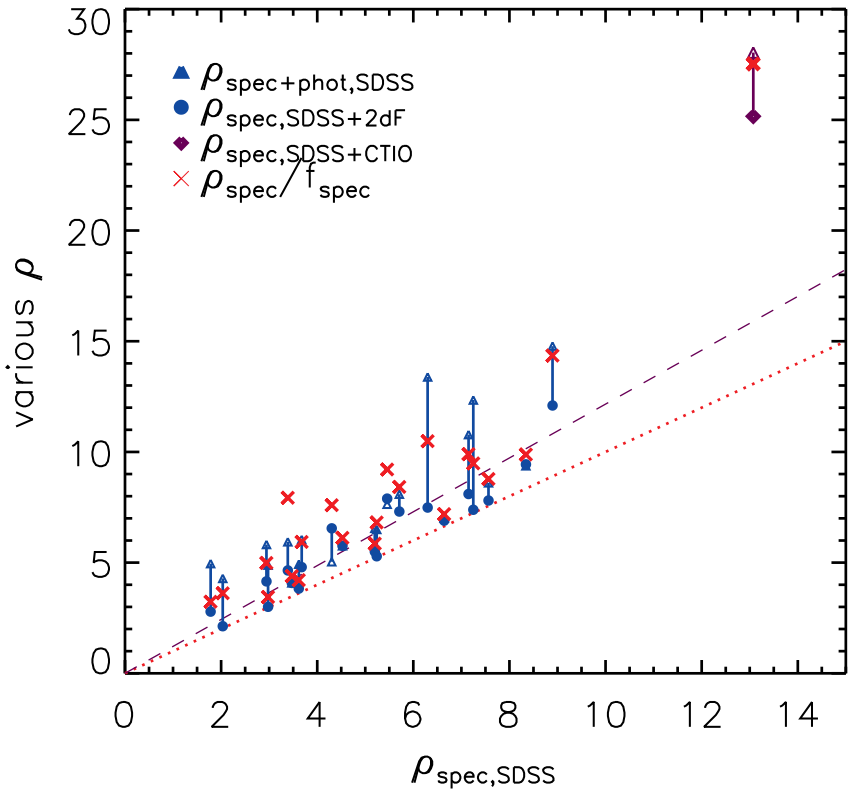

Figure 4.9: Comparison between the spectroscopy-only density measures (x axis) and various improved density measures (y axis). The solid triangles and circles show our spectro-photometric densities (ρ) and the spectroscopic densities based on the SDSS and 2dF database combined respectively. The purple diamond in the top right shows the spectroscopic density of Abell 2670 based on both the SDSS and our new CTIO database. The crosses show the result of rough correction for the incompleteness problem, using $\rho_{\rm spec}$ (i.e., x axis) and the completeness fraction $f_{\rm spec}$.

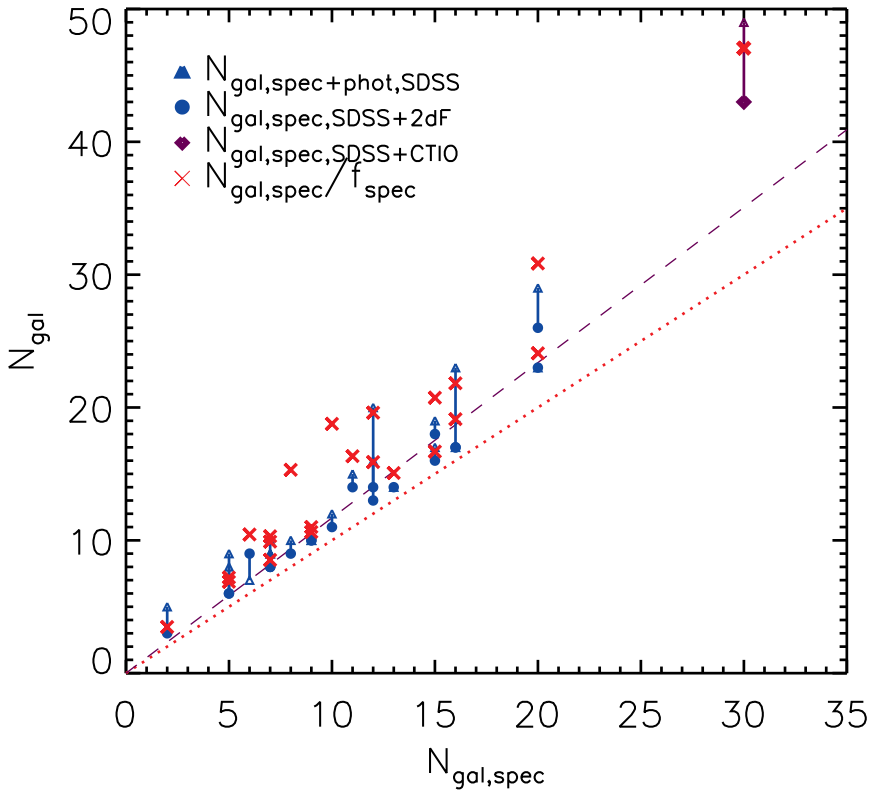

Figure 4.10: The same as Figure 4.9 but for the number of galaxies $N_{\rm gal}$. The dotted and dashed lines are the same as in Figure 4.8.

Chapter 5

A Demography in Galaxy Clusters

5.1 Galaxy Classification

5.1.1 Visual Inspection of Galaxy Morphology

Since Hubble classified galaxies by their morphology, galaxies with different morphology have been considered as distinct objects (Hubble, 1936). In order to see the characteristics of galaxies with their morphology, we need a method to classify galaxies. There are several ways to determine the galaxy morphology. For instance, physical parameters such as concentration index, *fracDev*, Gini parameter, and Sersic index are popular photometric methods (Goto et al., 2003; Capak et al., 2007). There are, however, many contaminants among galaxies for which morphology is determined by such photometric method. In order to minimize such contamination, we visually inspect 9426 member galaxies of clusters. We choose galaxies which are brighter than $r < 16.5$ to which

the visual inspection can be done with confidence. During the visual inspection, we also consider the *fracDev* values as a guide to the morphology. For self-consistency, we iterate the eye inspection several times and check whether the determined morphology is consistent. We rule out all galaxies with close companions because the companions interrupt us for get accurate photometric information such as colors and luminosities. Furthermore, galaxies with merger signatures are grouped separately for other studies and galaxies contaminated by saturated stars are rejected in the samples. As a result, we have early-type galaxies with round shapes and late-type galaxies with spiral patterns or blue disks.

5.1.2 Color Criterion for Red & Blue Galaxies

The colors of galaxies can be an indicator of galaxy morphology although they do not perfectly match each other. In order to divide galaxies by their color, we need to define the color cut which likely depends on the magnitude of galaxies. The color cut with a slope in the CMR plane is required for the classification. The color criterion is determined from the CMR shown in the Figure 5.1. We first plot all galaxies within a certain redshift range from the SDSS DR5 data. After finding the red-sequence through linear fit with 2σ clipping, we draw a dark-grey solid line indicating 3σ bluer than the red-sequence. The σ is a mean deviation of all points on the red-sequence from the linear fit. The galaxies above this line and those below the line are defined as red and blue galaxies respectively. We perform the same process for five redshift bins with the size of $\Delta z = 0.01$ in the range of $0.05 < z < 0.1$. This color criterion is consistent with that of Weimann et al. (2006) which is marked as a grey dashed line.

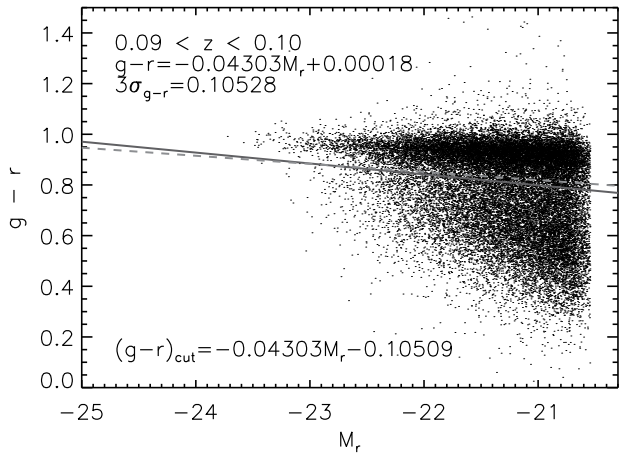

Figure 5.1: The color criterion is defined as a dark-grey solid line for galaxies between $0.09 < z < 0.1$. The line is determined from the red-sequence (see text for details). The galaxies above and below the line are defined as red and blue galaxies. The grey dashed line denotes the color cut from Weimann et al. (2006). Both lines show consistency.

5.2 Environment Effect on Cluster Galaxies

5.2.1 Benefit with the Catalog

There is a discussion concerning whether the environment has something to do with the photometric properties including galaxy luminosities and colors. Since our catalog is extracted from the nearly complete and homogeneous dataset of the SDSS, we study the environmental effect on cluster galaxies with relatively unbiased samples.

Many previous studies were based on how galaxy properties change with the environment parameters (Dressler, 1980; Postman & Geller, 1984; Goto et al., 2003; Capak et al., 2007; Park et al., 2007; van Dokkum & Quadri, 2007; Sorrentino, & Rifatto, 2007). However, the galaxies in the outskirts of rich clusters and those in the centers of poor clusters should not be regarded as the same even though they have the same local density because their evolution history would be very different. The central galaxies of small clusters dominate in their regions, and thus they undergo different evolution history. Therefore, we study the clustocentric dependence of colors and luminosities in each cluster. For more reliable statistics, we stack clusters with a similar density and compare the characteristics of the member galaxies of clusters with clustocentric radius scaled in the virial radius of each galaxy cluster.

Although our catalog considers the additional members selected by the CMR, we choose only the spectroscopic member galaxies of clusters for the clustocentric dependence study. Because the CMR method targets ETGs, the sample can be biased if we take into account photometric member galaxies too. Hence, they are excluded from this clustocentric dependence study.

5.2.2 Clustocentric Dependence of Luminosities and Colors in Clusters

We look into galaxy properties with clustocentric radius of clusters within density bins. The physical parameters such as the virial radius are defined in 2-dimension since they are estimated with spectroscopic+photometric member galaxies. The 3-d distance is not always better than the projected one because of the finger-of-god effect. Therefore, we use projected radius. The virial radius mean the distance to which galaxies are under the influence of a galaxy cluster. We see galaxy luminosities and colors going to $4R_{200}$ to check how far the galaxy properties is dependent of clustocentric radius, if any. If the properties show reliance far beyond the virial radius, the definition of the virial radius of this study should be revised.

Figure 5.2 – 5.6 show the galaxy colors and luminosities dependence with the clustocentric radius. We first select the richest clusters with $\rho > 20$ and then divide the rest into equal number bins. The median values are denoted as the solid lines and the 25% and 75% quartiles are presented as the dashed lines. Statistically, there seems to be no color or magnitude dependence in the panels (a), (c). However, within the virial radius R_{200}, there is slight color change as a function of the clustocentric radius for blue galaxies indicated as the 25% dashed line in the panel (a). Moreover, the magnitude increases in the cluster centers shown as the 75% dashed line in the panel (c). When we separate the galaxies with their morphology (the panels (b), (d)), we see no clustocentric dependence within the virial radius. This implies that the color dependence of the blue galaxies is due to the fact that the fraction of blue galaxies increases as we see the cluster outskirts which is called the *morphology-density relation* (MDR). The

magnitude of the cluster galaxies also reveal a shallow increment for luminous galaxies (the upper dotted lines in panels (c)) as we go to the center within R_{200} and this is mainly due to the increase of the luminosity of early-type galaxies (the red dotted lines in (d)). This phenomenon is plausible since there are a larger number of bright ETGs in cluster central regions. For the densest clusters (Figure 5.2) such magnitude increment is not shown and this could be due to the small number of galaxies in Figure 5.2 compared with Figure 5.3 – 5.6.

Another aspects of the member galaxies are investigated in the Figure 5.7 – 5.11. Instead of the median color and magnitude, we see the fraction of galaxies with a certain morphology or color. The morphology and color of galaxies are determined as in §5.1 and clusters are stacked with their densities as explained above. The fraction of early-type galaxies decreases as a function of radius whereas the fraction of late-type galaxies (LTGs) increases. This tendency disappears beyond the virial radius and this is consistent with the definition of the virial radius. The densest clusters in Figure 5.7 show relatively large errors compared with the other clusters due to the small number of galaxies in the clusters. The number ratios between red and blue galaxies show a similar trend, too. The bottom panels (d), (e), (f) of Figure 5.7 – 5.11 present the ratio of ETGs (red) to LTGs (blue), and this ratio shows the radial trends more clearly, as shown in the top panels.

The panels (c), (f) of each figure show the number ratios of red ETGs and blue ETGs. There is no clear clustocentric dependence and this implies that the color dependence with the radius of morphologically selected galaxies in clusters is ignorable. In other words, the radial trend of the fraction of galaxies with a certain color could be caused mostly by the MDR. The MDR seems to be a

fundamental relation whereas the color-density relation is a secondary effect of the MDR.

The clustocentric dependence of the ratios of ETGs to LTGs for five cluster density bins show continuous trend in their values and slopes (see Figure 5.12). The ratios are higher and the slopes are steeper for denser clusters within the virial radius. The red and blue galaxy ratios also reveal a similar tendency. The MDR effect is present in both rich and poor clusters but stronger for denser clusters. The galaxies in denser clusters could undergo more vigorous environmental effects through merging and interacting events, and thus the stronger MDR would be due to more robust effects in harsher environments.

The figures include neighbor galaxies extended out to $4R_{200}$. Generally, the radial trend is strong within $1R_{200}$. Within $2R_{200}$, the tendency is not as clear as in $1R_{200}$ but still remains and it vanishes away beyond $2R_{200}$. This implies that the virial radius is reliably defined.

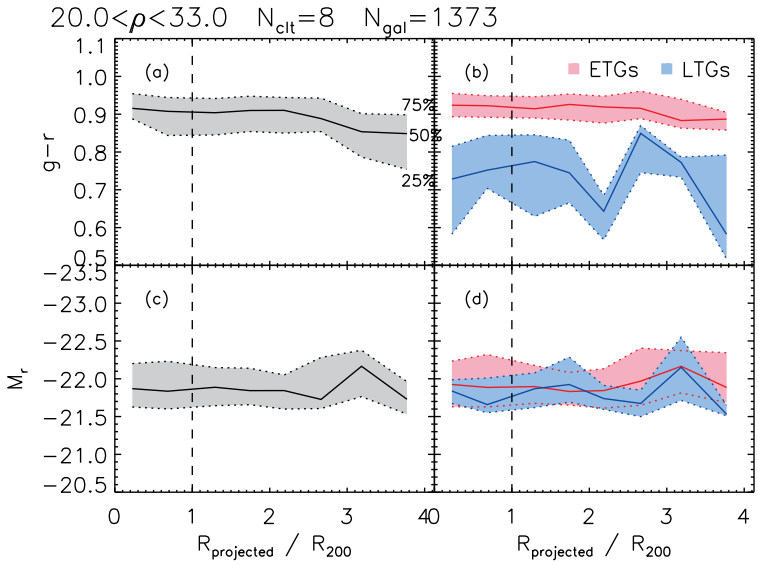

Figure 5.2: The clustocentric dependence of the colors and luminosities of member galaxies of clusters. The clusters are stacked for the better statistics. The clustocentric radius are scaled in the virial radius of each cluster. The solid lines are the median values of the color and magnitude and the dotted lines denote the 25% and 75% quartiles. The dashed lines indicate the virial radius. The left panels (a), (c) are for all galaxies in clusters and the right panels (b), (d) show the galaxies separated by their morphology with the early-type (red lines and pink shaded regions) and the late-type (blue lines and blue shaded regions) galaxies. There is little clustocentric dependence both in color and magnitude. The density range of clusters, the number of clusters, and the number of member galaxies of clusters within virial radius are presented above of the panels.

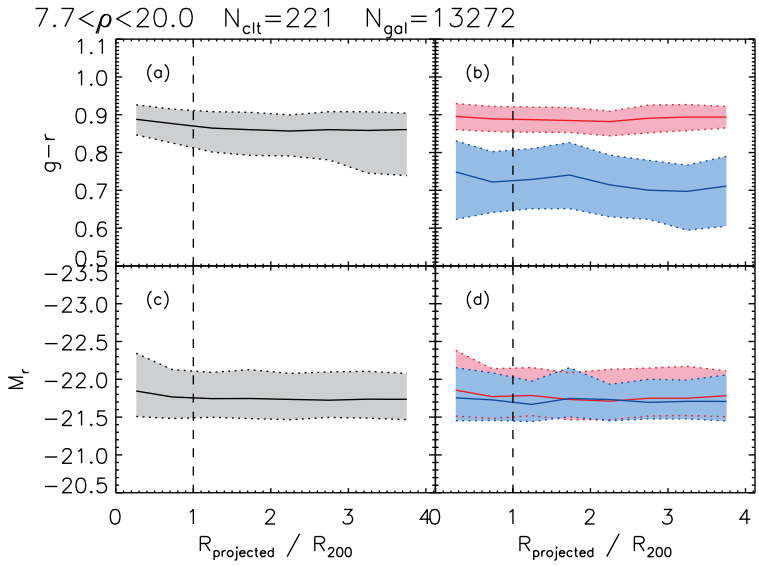

Figure 5.3: The same as Figure 5.2 but in the different density bin.

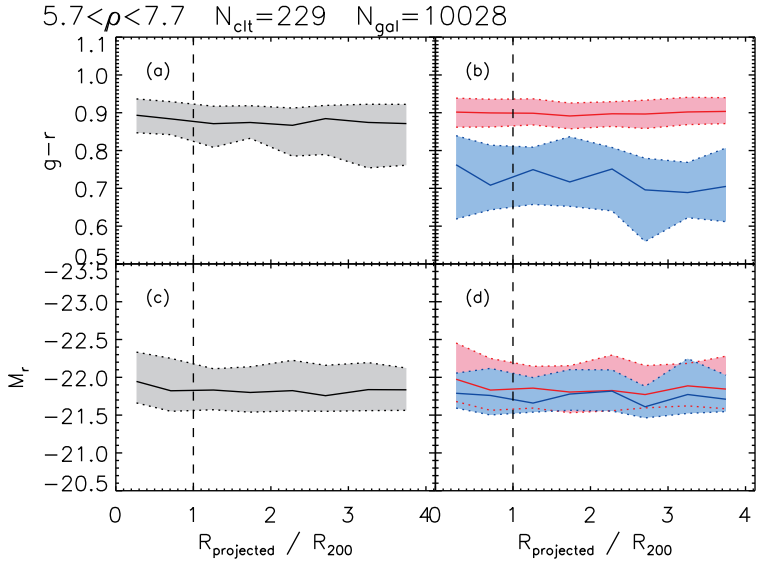

Figure 5.4: The same as Figure 5.2 but in the different density bin.

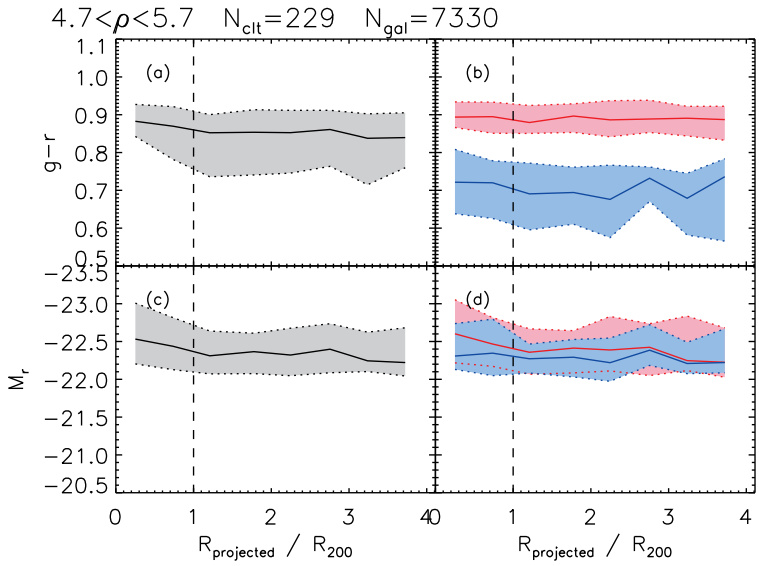

Figure 5.5: The same as Figure 5.2 but in the different density bin.

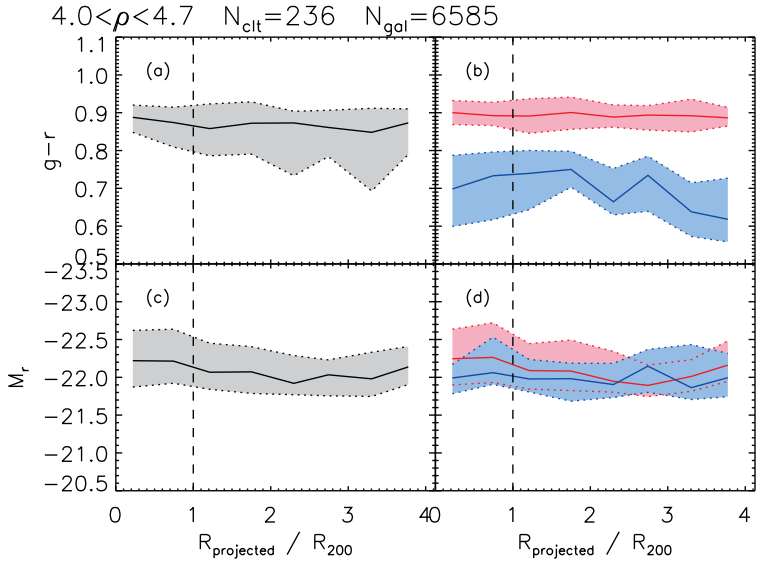

Figure 5.6: The same as Figure 5.2 but in the different density bin.

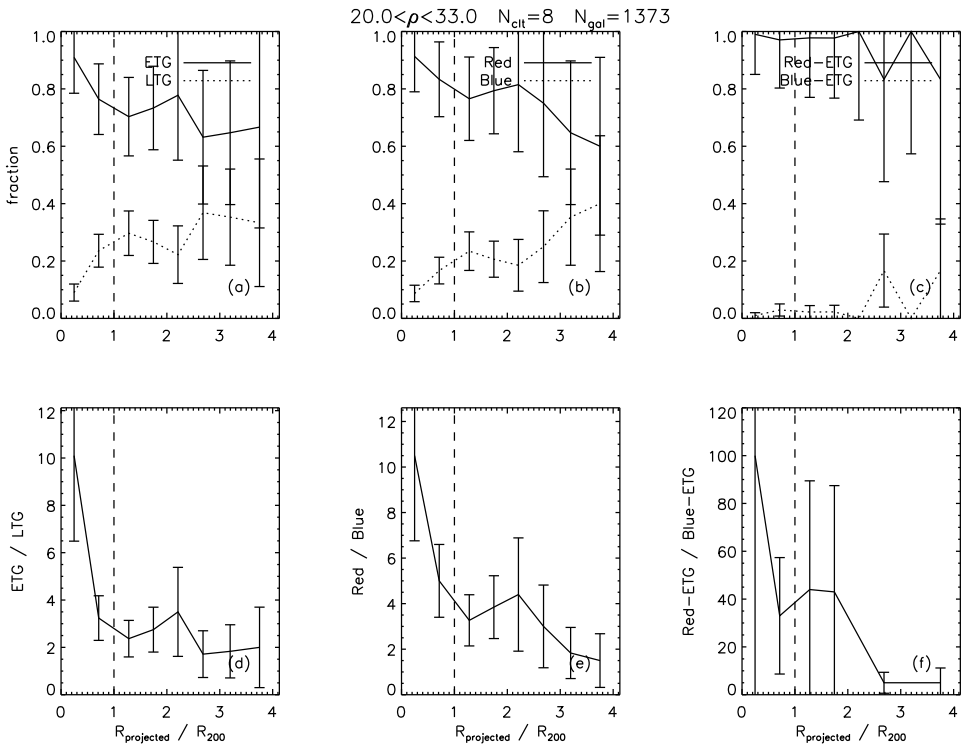

Figure 5.7: The fractions of galaxies selected by their morphology and color show clear clustocentric dependence. The solid and dotted lines denotes ETGs and LTGs respectively. The dashed lines indicate the virial radius. The left panels (a), (d) reveal the fraction of ETGs and LTGs, the middle panels (b), (e) show the fraction of red and blue galaxies, and the right panels (c), (f) present the fraction of red ETGs and blue ETGs. The bottom panels (d), (e), (f) shows the ratio of ETGs to LTGs, red to blue galaxies, and red ETGs to blue ETGs respectively. There is a clear clustocentric dependence indicating the morphology-density relation except in the right panels (c), (f).

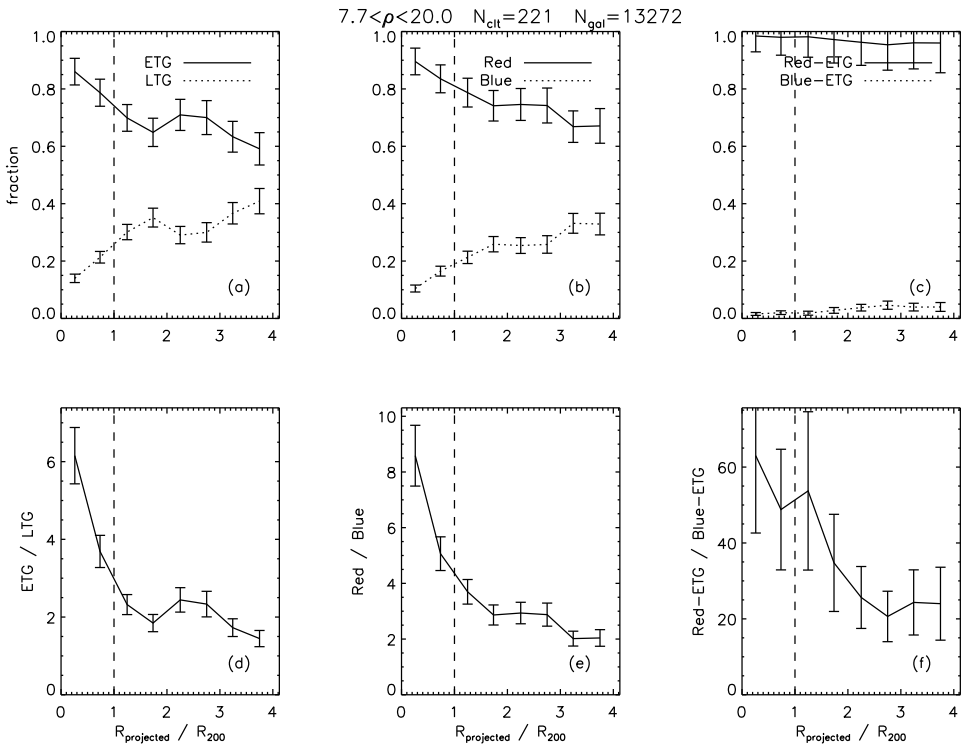

Figure 5.8: The same as Figure 5.7 but in the different density bin.

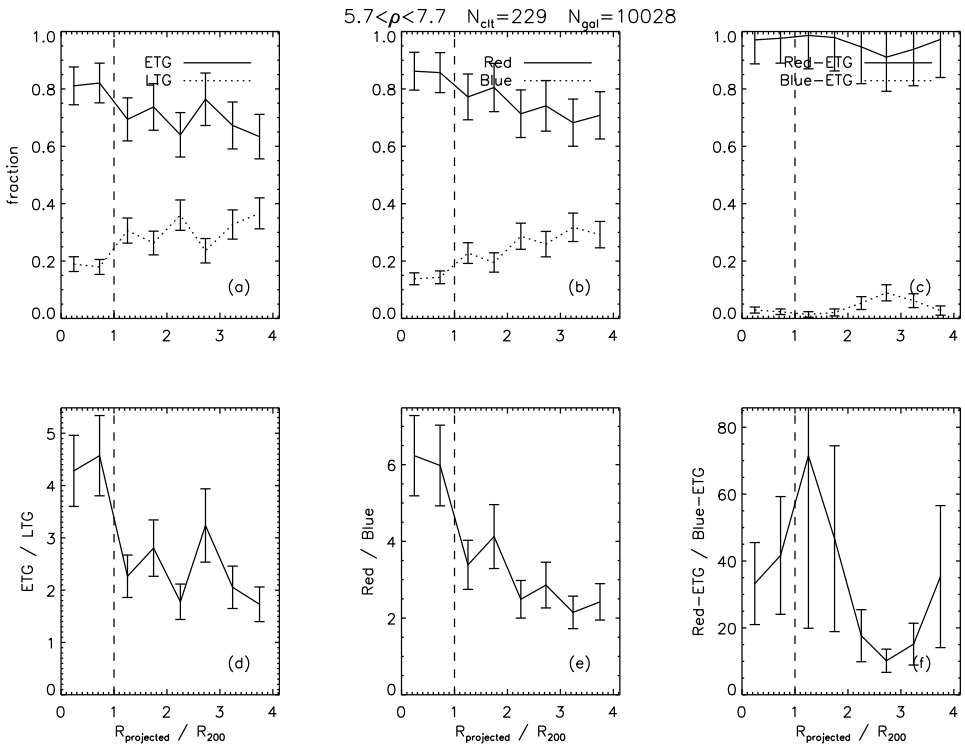

Figure 5.9: The same as Figure 5.7 but in the different density bin.

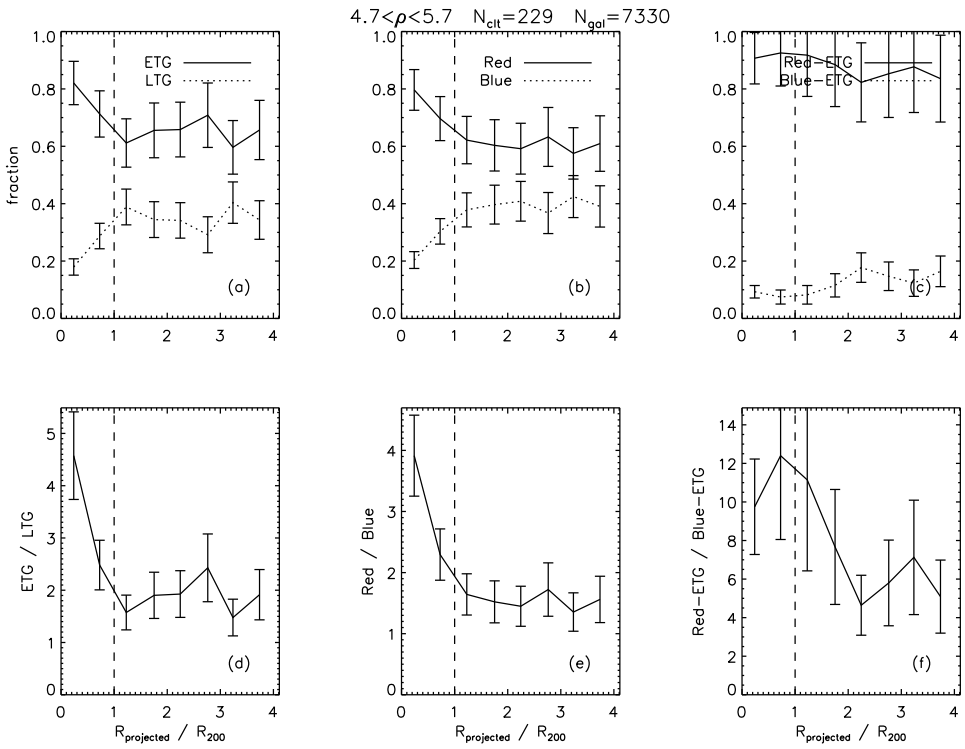

Figure 5.10: The same as Figure 5.7 but in the different density bin.

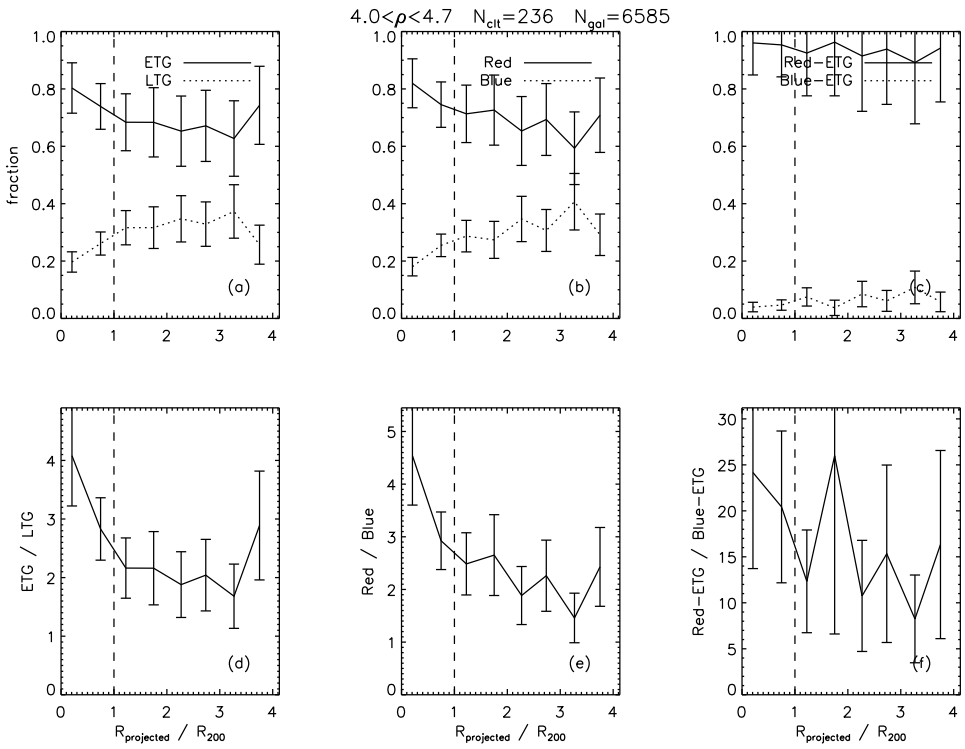

Figure 5.11: The same as Figure 5.7 but in the different density bin.

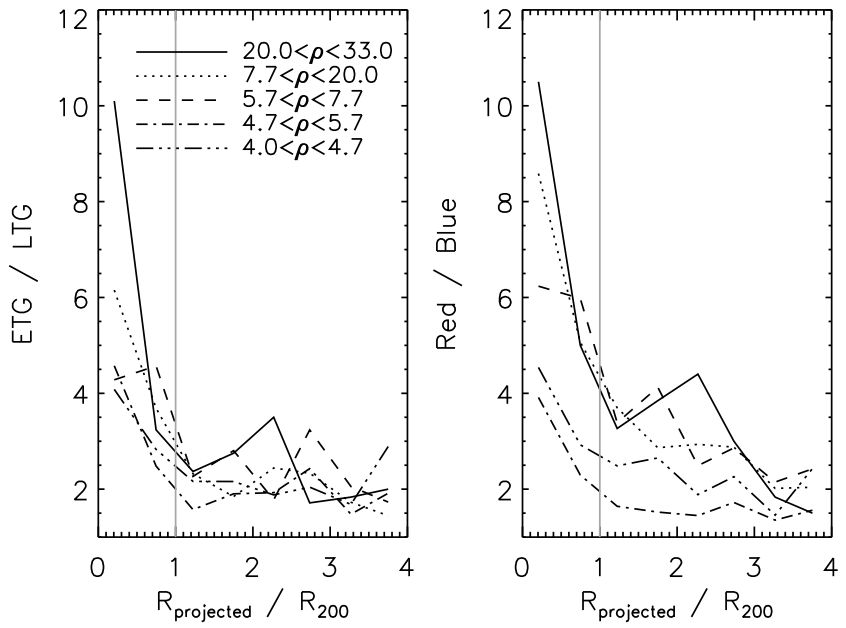

Figure 5.12: In the left panel, the ratios of ETGs to LTGs for five cluster density bins are shown. Different lines indicate different density of clusters and the vertical-grey lines imply the virial radius. The ratios decrease with the clustocentric radius and the ratios are higher and their slopes are steeper for denser clusters. The right panel shows the ratios of red to blue galaxies and they reveal the similar tendency to the left panel.

5.3 Brightest Cluster Galaxies in Clusters

BCGs are centrally located in clusters so that they are the worst samples having the serious incompleteness problem due to the fiber collisions. This incompleteness results in unreliable density measurement and prevents us from studying whether the characteristics of BCGs result from the environment or not. Since our new spectro-photometric density minimizes the incompleteness problem, it is a robust tool to study the environmental effect on BCG properties.

The BCGs are simply selected from our cluster catalog as the "brightest" member galaxy in each cluster. Early-type BCGs are chosen and BCGs with close companions are rejected through the visual inspection since the companion galaxies interrupt to get accurate photometric information. We now have 689 BCGs and the local density dependence of the BCG magnitude and color is presented in Figure 5.13. The solid lines denote the median value and the dashed lines indicate 25% and 75% quartiles. The magnitude and color of the BCGs have the positive correlation with the galaxy local density in the top panels. The BCGs in denser environments are brighter and redder. The CMR can explain the fact that the slope of color is not as clear as that of magnitude in that the color spans smaller scale than the magnitude does in the CMR. If the BCG magnitude is dependent of its local density, this can cause the color dependence on the density due to the CMR and vice versa. In order to disentangle such degenerate density dependence of colors and luminosities, we investigate the magnitude-density dependence at given narrow color ranges and the color-density reliance at given magnitude ranges. The top panels are with all BCGs and the others are divided into equal-number bins for the color and the magnitude. The magnitude depends on the density in an entire color range. This dependence still remains

within the narrow color ranges shown in the column (a). On the other hand, the color-density dependence vanishes away at given magnitude ranges shown in the column (c). The luminosities of BCGs positively correlate with the local density being independent of their colors. Therefore, we conclude that BCGs residing in the denser environments are more luminous than those in the less dense regions while the colors of BCGs in rich clusters is indistinguishable with those of BCGs in the intermediate or poor clusters.

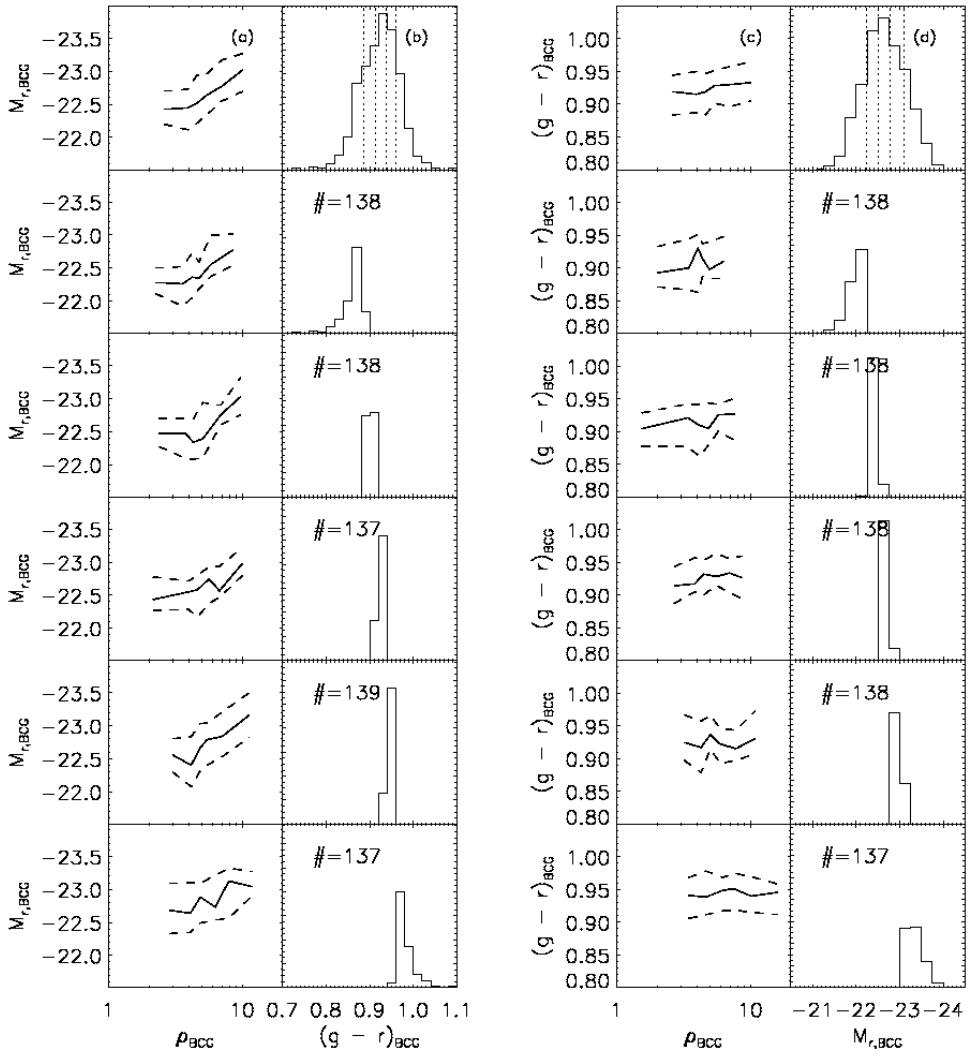

Figure 5.13: The magnitude-density and the color-density relation of BCGs. The solid lines present the median of magnitudes and colors and the dashed lines denote 25% and 75% quartiles in the column (a), (c). The dotted lines in the column (b), (d) show the boundaries of the equal-number bins. The number of samples of each bin is shown in the column (b), (d). The top panels are for all BCGs and the others are within the bins. The magnitudes at given color ranges depend on the local density while the colors do not.

We try to check the difference between BCGs and non-BCGs in our cluster sample. To answer the question of whether BCGs are intrinsically different objects with other giant ellipticals, we compare the magnitude-density relation of the BCGs to the second and third brightest cluster galaxies (2nd, 3rd BCGs) in Figure 5.14 and Figure 5.15. We can see the dependence between the luminosity and density in both 2nd and 3rd BCGs and they do not seem to be different with BCGs. For the statistical comparison of the density dependence, we use the "bootstrap" technique. At first we make linear fit of all BCGs and 2nd BCGs respectively in the column (a), and the slopes for all data are indicated as dot-dashed lines in the column (c). After that, we randomly resample from BCGs and 2nd BCGs with the same size as the original population. Some of them might be included several times. And then, we find the slopes of fit with these resampled data. We iterate 10 000 comparison and the distribution of the slopes of the resampled data is shown in the column (c). The horizontal thick lines denote the 1-sigma errors which are estimated from the cumulative distribution of the slopes. The 3rd BCGs are compared with the BCGs through the same process. BCGs, 2nd BCGs, and 3rd BCGs have no systematic difference in their magnitude-density dependence within 1σ confidence level. In this regard, BCGs do not seem to be special compared with other luminous elliptical galaxies because their magnitude-density dependence are not distinct each other.

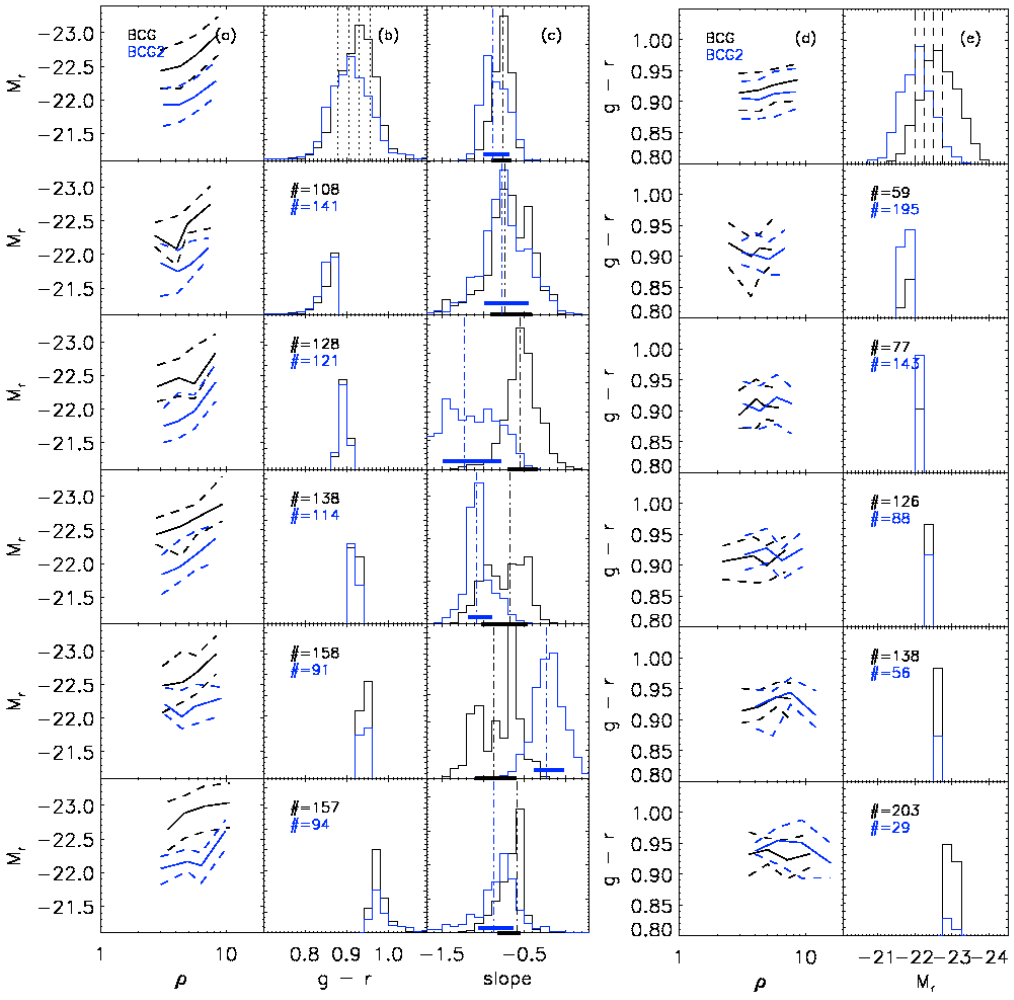

Figure 5.14: The format is the same as Figure 5.13. We compare the density dependence of the magnitude and color of BCGs and 2nd BCGs. In the column (c), the slope distributions of the magnitude-density relation are added. This distribution is derived from the bootstrap test. The black lines are from BCGs and the blue lines are from 2nd BCGs. The thick horizontal black and blue lines in the column (c) shows the 1σ errors.

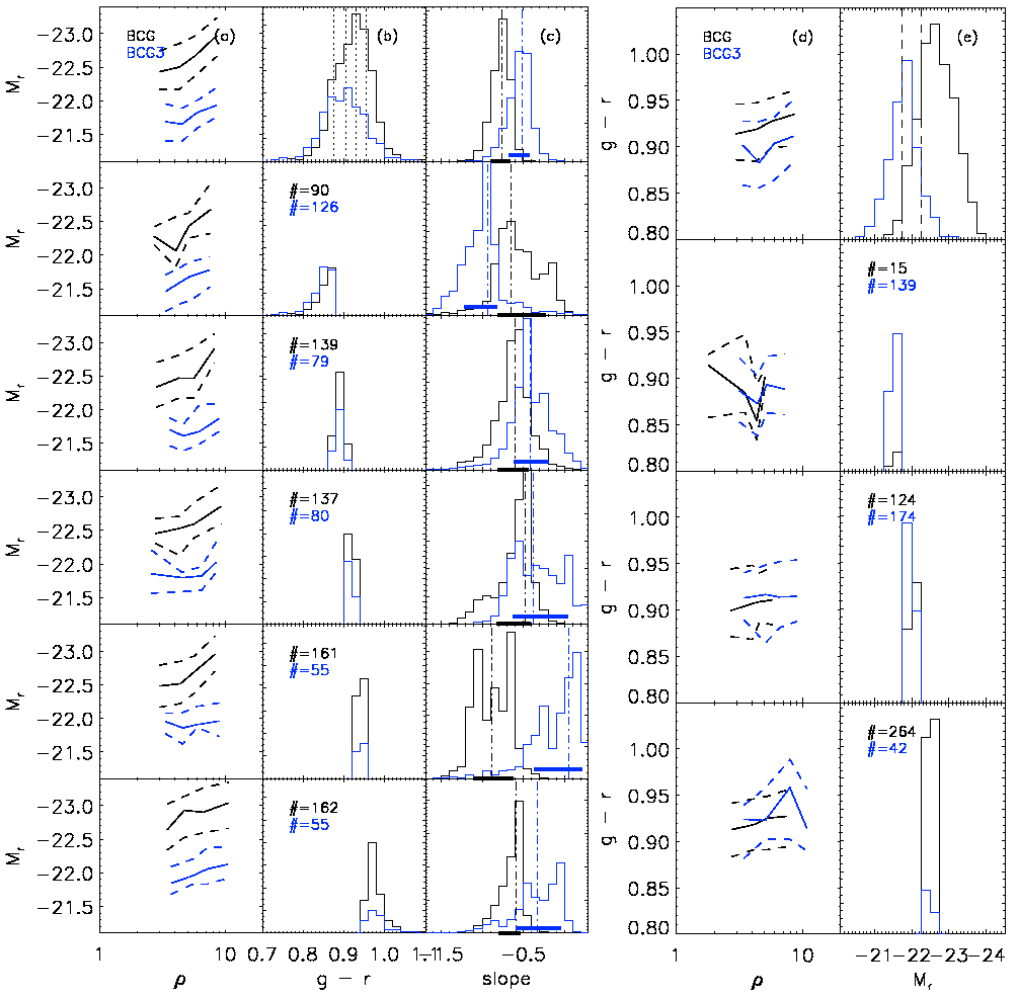

Figure 5.15: The same as Figure 5.14 but comparison of BCGs and 3rd BCGs.

5.4 Cluster Galaxies vs. Non-cluster Galaxies

Cluster galaxies experience different evolution history with galaxies in the field. With our density measurement method, we could find galaxies in sparse regions and compare them to member galaxies of clusters. For the comparison, we choose 4521 non-cluster galaxies (hereby, NCGs) for which the density is $\rho = 0$. This does not always mean that they are field galaxies because our galaxies used for density estimation are volume-limited samples that are brighter than $M_{\rm r} = -20.55$. The NCGs simply have no luminous galaxies as their close neighbors. They can be a field galaxy, the central galaxy of a small group, the brightest galaxy of a fossil group, and so on. We perform eye-inspection for the NCGs as explained in §5.1.1.

Figure 5.16 show the luminosity and color distributions of BCGs and NCGs galaxies. Brighter galaxies are generally redder than fainter galaxies, we try to see the color difference in the same magnitude ranges. The general bin size is $\Delta M_{\rm r} = 0.25$ but we stack 2 – 3 bins when the sample number is small. When we see the color distribution of galaxies in each magnitude bin, the mean color of the NCGs is bluer than that of the BCGs. Thus, NCGs are bluer than BCGs when they have the same magnitude. The Kolmogorov-Smirnov test (KS test) tells that BCGs and NCGs are significantly different population with about 80% confidence level ('P' values in the column (b) of the Figure 5.16). For the better statistics, we perform the "bootstrap" test as described in Rogers et al. (2007). We do 10 000 comparison between the sub-samples from BCGs and NCGs (blue lines). For the comparison, we perform the same process of the two sub-samples both obtained from the BCGs (red lines). The column (c) of the Figure 5.16 is the distributions of the confidence level of the KS statistics.

Some of them show discrete distributions owing to the small sample number. When the sub-samples are obtained from the same distribution, KS statistics shows roughly uniform distribution in their 'P' values. On the contrary, the 'P' value is close to zero when two distributions come from different populations. The comparison between BCGs and NCGs shows a strongly-positively skewed distribution implying that they are different populations. The median of the 'P' values (dot-dashed lines in the column (c)) which is close to zero and the distributions of the 'P' values present that BCGs and NCGs come from distinct populations.

We compare 2nd BCGs and 3rd BCGs to NCGs in Figure 5.17 – 5.18. The NCGs are bluer than 2nd and 3rd BCGs, too. We perform the same test as BCGs and NCGs. The 2nd and 3rd BCGs seem to originate from different populations with NCGs.

It is debated whether mass or environments is the primary factor that affects galaxy colors (Pimbblet et al., 2002; Balogh et al., 2004b; Tanaka et al., 2004; Koo et al, 2005). As shown in this section, although we choose galaxies with the similar luminosity meaning the similar stellar mass, cluster galaxies and non-cluster galaxies seem to be derived from distinct populations. The clear difference between them is what kind of environment that they live in. Hence, galaxies even with the same stellar mass show different colors relying on their environments.

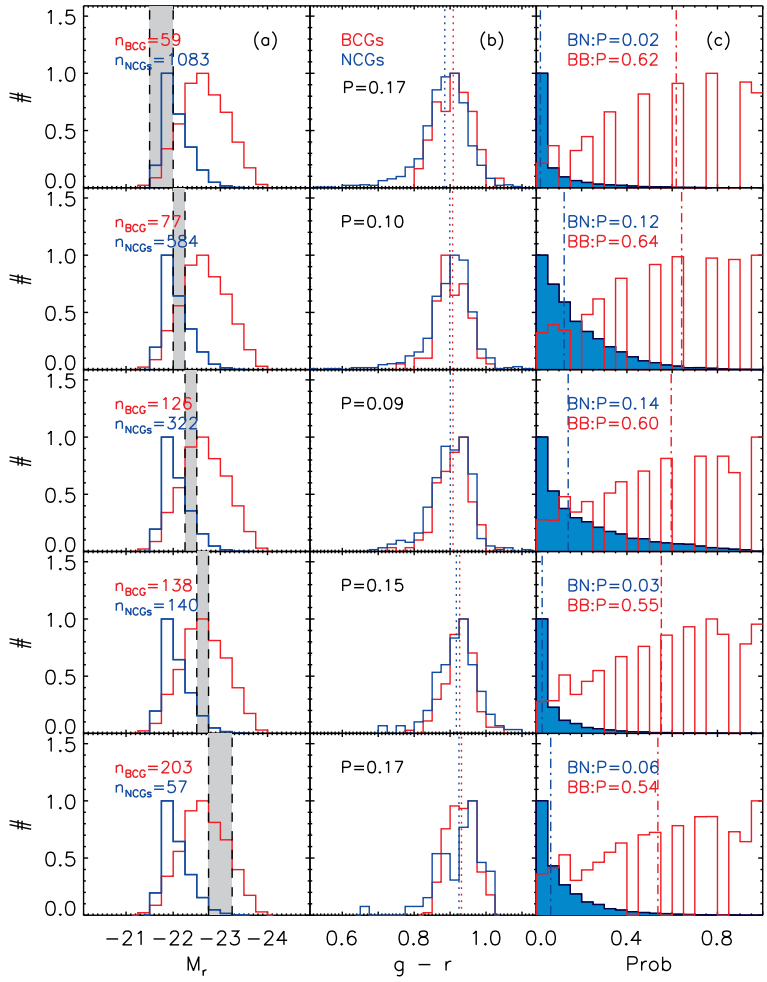

Figure 5.16: The luminosities and colors of BCGs and NCGs are compared. The red and blue lines present BCGs and NCGs respectively. The grey-shaded regions indicate the boundary of bins and the number of galaxies in each bin is marked in the column (a). The color distributions of galaxies in each bin are presented in the column (b) and the dotted lines are the mean color. The dot-dashed lines in the column (c) denote the median confidence level of the KS test. 'BN' denotes the comparison between the sub-samples from the BCGs and NCGs and 'BB' means the comparison of two distinct sub-samples obtained from BCGs. The distribution of 'P' values show the marked difference between BCGs and NCGs.

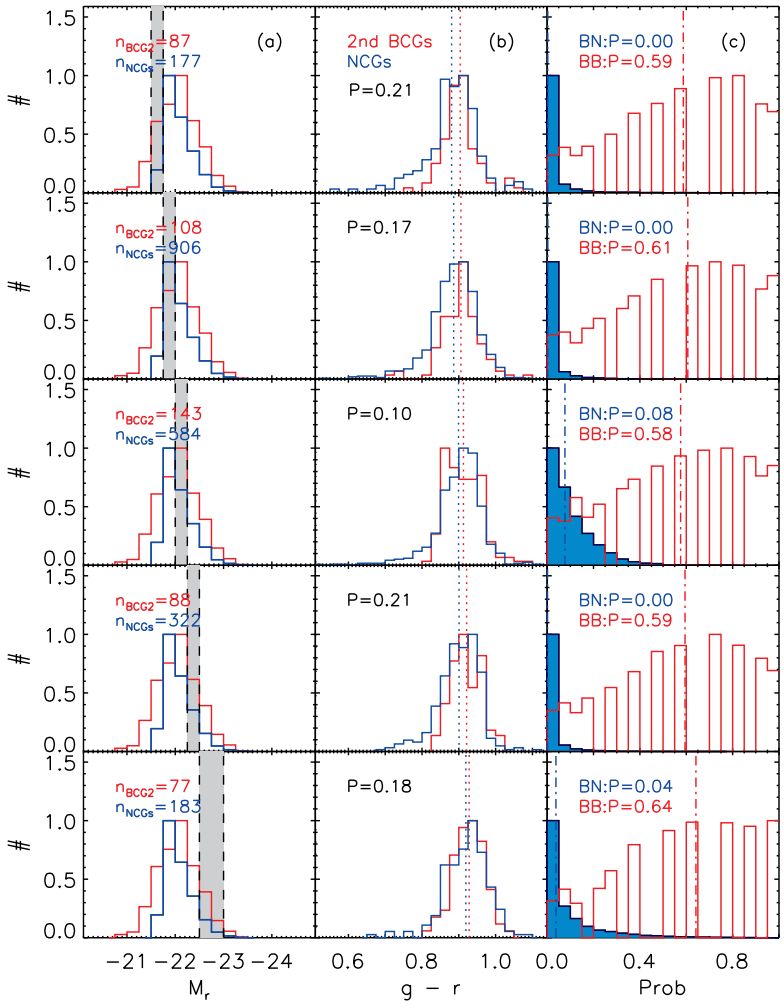

Figure 5.17: The same as Figure 5.16 but comparison of 2nd BCGs and NCGs.

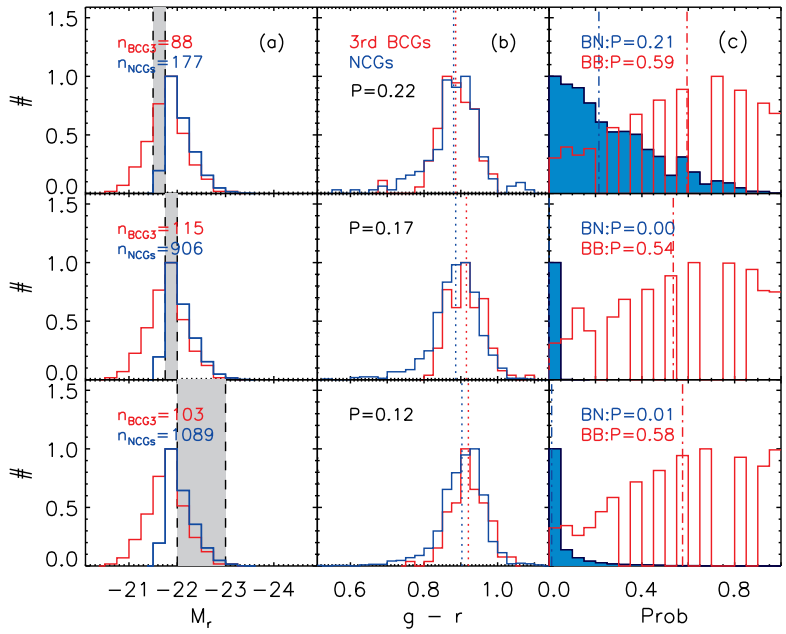

Figure 5.18: The same as Figure 5.16 but comparison of 3rd BCGs and NCGs.

Chapter 6

Summary and Discussion

We develop and test a method for finding galaxy clusters in the SDSS spectroscopic and photometric database. Our method improves over the previous density measurements solely based on the spectroscopic surveys by finding additional cluster member candidates via the color-magnitude relation technique. The problem of spectroscopic incompleteness due to fiber collisions in dense fields is minimized in our method. The member galaxies selected by the color-magnitude relation lead to a satisfactory completeness and purity. Hence, our additional member selection is reliable without redshifts and relatively free from the projection effect. Moreover, the CTIO observation supports that our new spectro-photometric density represents more realistic measurement for dense clusters.

With this spectro-photometric density measurement, we find 924 galaxy clusters of which 212 are new. We provide a catalog of these clusters including important properties such as the virial radius, velocity dispersion, and richness parameters. The density we estimate is in good agreement with the properties

relating to the cluster mass and size. We also provide an estimating scheme for our spectro-photometric density measure simply using the spectroscopic completeness rate.

Our new density and cluster catalog are robust in the following aspects.
(1) Our density contains not only the information of the number density but also the information of the concentration of galaxies by considering the distance to each neighboring galaxy.
(2) It minimizes the incompleteness problem in dense environments.
(3) Our catalog includes a large number of galaxy clusters and their member galaxies with high completeness and homogeneity.

Therefore, our new density information on galaxy clusters is useful for the study of the environmental effect on the galaxy evolution.

In clusters, the median colors and magnitudes show no clustocentric dependence. However, the blue and bright end of galaxies reveal a slight dependence within the virial radius. This clustocentric dependence seems to result from the morphology-density relation because the dependence becomes ambiguous when we separate the galaxies with their morphology. The fraction of early-type galaxies decreases with the clustocentric radius while that of the late-type galaxies increases. The red and blue galaxy fractions also show the same trend. This dependence seems to be caused by the MDR, too. When we compare the fractional dependence in clusters with the different density, denser clusters show a higher ratio of ETGs (red) to LTGs (blue) and a stronger clustocentric dependence. This tendency seems to be generated by the environmental effect on the morphology of galaxies. The morphology-density relation is omnipresent in rich and poor clusters. However, dense, harsh environments contain a larger number of

early-type galaxies, meaning a clearer morphology-density relation. The galaxies in such severe environments could have experienced the mechanisms that can transform the galaxy morphology such as ram pressure stripping, tidal stripping, or major merger more frequently in their formation history. In sum, the galaxies in cluster show the following.

(1) The median color and magnitude have no correlation with the clustocentric radius.

(2) The fraction of early-type galaxies increases at cluster centers whereas that of late-type galaxies declines.

(3) The dependence between the galaxy color and clustocentric radius is attributed to the morphology-density relation.

(4) The morphology-density relation is stronger in dense clusters.

We also study 689 BCGs in our catalog by analyzing their photometric properties such as colors and luminosities. We conclude the following facts.

(1) BCGs in denser environments are more luminous than those in less dense regions.

(2) Cluster galaxies including the 2nd and 3rd BCGs show the same magnitude-density dependence.

(3) Non-cluster galaxies have bluer color compare with cluster galaxies.

BCG luminosities and colors have a positive relation with local density. The BCGs in denser regions are more luminous and slightly redder than those in sparse regions. While this trend of color vanishes within the narrow magnitude ranges, the magnitude slope remains even in the small color ranges. We conclude that the color-density relation arises from the magnitude-density relation and the CMR. In other words, the luminosities of BCGs grow with the local density

without color change. There should be more careful test but the dry merger might be one of the possibilities since it increases the luminosity without affecting their colors through the galaxy formation history. Other cluster galaxies such as the 2nd and 3rd brightest galaxies also show a similar dependence on their local density. BCGs do not seem to be distinct objects with other cluster galaxies in terms of their magnitude-density relation.

We also argue that cluster galaxies and non-cluster galaxies have different natures in their color. NCGs are usually bluer than cluster galaxies at a given magnitude. Thus, environment plays a role in determining galaxy colors. Environmental effect that regulate the star formation in cluster galaxies by stripping the gas can cause such color difference.

Further studies on the star-formation rate and the metallicity dependence in the clusters and other BCG properties such as line indices, fundamental plane, and merger signature are required to unravel the formation and evolution history of cluster galaxies and brightest cluster galaxies.

Bibliography

Abadi, M. G., Moore, B., & Bower, R. G. 1999, MNRAS, 308, 947

Abell, G. O. 1958, ApJS, 3, 211

Abell, G. O., Corwin, H. G., & Olowin, R. P. 1989, ApJS, 70, 1

Bahcall, N. A. et al. 2003, ApJS, 148, 243

Balogh, M. et al. 2004a, MNRAS, 348, 1355

Balogh, M. L., Baldry, I. K., Nichol, R., Miller, C., Bower, R., & Glazebrook, K. 2004b, ApJ, 615, L101

Baum, W. A. 1959, PASP, 71, 106

Beers, T. C., Flynn, K., & Gebhardt, K. 1990, AJ, 100, 32

Bekki, K. 1999, ApJ, 510, L15

Binggeli, B., Tammann, G. A., & Sandage, A. 1987, AJ, 94, 251

Blanton, M. R. et al. 2003a, AJ, 125, 2276

Blanton, M. R. et al. 2003b, AJ, 125, 2348

Blanton, M. R., Eisenstein, D., Hogg, D. W., Schlegel, D. J., and Brinkmann, J. 2005, ApJ, 629, 143

Boselli, A. & Gavazzi, G. 2006, PASP, 118, 517

Byrd, G. & Valtonen, M. 1990, ApJ, 350, 89

Carlberg et al. 1997, ApJ, 485, L13

Capak, P. et al. 2007, ApJS, 172, 284

Christlein, D. & Zabludoff, A. I. 2005, ApJ, 621, 201

Chung, A., van Gorkom, J. H., Kenney, J. D. P., & Vollmer, B. 2007, ApJ, 659, L115

Colless, M. et al. 2001, MNRAS, 328, 1039

Croft, R. A. C., Dalton, G. B., Efstathiou, G., Sutherland, W. J., & Maddox, S. J. 1997, MNRAS, 291, 305

Croton, D. J. et al. 2005, MNRAS, 356, 1155

Dalton, G. B., Efstathiou, G., Maddox, S. J., & Sutherland, W. J. 1994, MNRAS, 269, 151

Dressler, A. 1980, ApJ, 236, 351

Dressler, A. et al. 1997, ApJ, 490, 577

Elbaz, D. et al. 2007, A&A, 468, 33

Fabian, A. C., 1994, ARA&A, 32, 277

Farouki, R. & Shapiro, S. L. 1980, ApJ, 241, 928

Fujita, Y. & Nagashima, M. 1999, ApJ, 516, 619

Gallagher, J. S., Ostriker, J. P., 1972, AJ, 77, 288

Giovanelli, R. G., Haynes, M. P., & Chincarini, G. L. 1986, ApJ, 300, 77

Gisler, G. R. 1978, MNRAS, 183, 633

Gladders, M. D. & Yee, H. K. C. 2000, AJ, 120, 2148

Gomez, P. L. et al. 2003, ApJ, 584, 210

Goto, T. et al. 2003, MNRAS, 346, 601

Gunn, J. E. & Gott, J. R. 1972, ApJ, 176, 1

Hansen, S. M., McKay, T. A., Wechsler, R. H., Annis, F., Sheldon, E. S., & Kimball, A. 2005, ApJ, 633, 122

Hogg, D. W. et al. 2004, ApJ, 601, L29

Hubble, E. P. 1936, "The Realm of the Nebulae.", Yale University Press

Icke, V. 1985, A&A, 144, 115

Katgert, P., Biviano, A., & Mazure, A. 2004, ApJ, 600, 657

Kim, R. S. J. et al. 2002, AJ, 123, 20

Kochanek, C. S. et al. 2003, ApJ, 585, 161

Koo, D. C. et al. 2005, ApJ, 634, L5

Larson, R. B. & Tinsley, B. M. 1978, 219, 46

Larson, R. B., Tinsley, B. M., & Caldwell, C. N. 1980, 237, 692

Lewis, I. et al. 2002, MNRAS, 334, 673

Lin, Y.-T., Mohr, J. J., & Stanford, S. A. 2004, ApJ, 610, 745

Liu, F. S., Xia, X. Y., Mao, S., Wu, H., & Deng, Z. G. 2007, MNRAS in press, (astro-ph/0712.0927)

López-Cruz, O., Barkhouse, W. A., & Yee, H. K. C. 2004, ApJ, 614, 679

Lumsden, S. L., Nichol, R. C., Collins, C. A., & Guzzo, L. 1992, MNRAS, 258, 1

Makino, J. & Hut, P. 1997, ApJ, 481, 83

Matthews, T. A., Morgan, W. W., & Schmidt, M. 1964, ApJ, 140, 35

Merritt, D. 1985, ApJ, 289, 18

Miller, C. J. et al. 2005, AJ, 130, 968

Moore, B., Katz, N., Lake, G., Dressler, A., & Oemler, A. 1996, Nature, 379, 613

Moore, B., Lake, G., Quinn, T., & Stadel, J. 1999, MNRAS, 304, 465

Navarro, J. F., Frenk, C. S., & White, S. D. M. 1996, ApJ, 462, 563

Oegerle, W. R. & Hill, J. M. 2001, AJ, 122, 2858

Ostriker, J. P. & Tremaine, S. D., 1975, ApJ, 202, L113

Ostriker, J. P. & Hausman, M. A., 1977, ApJ, 217, L125

Park, C., Choi, Y.-Y., Vogeley, M. S., Gott, J. R., & Blanton, M. R. 2007, ApJ, 658, 898

Pimbblet, K. A. et al. 2002, MNRAS, 331, 333

Postman, M. & Geller, M. J. 1984, ApJ, 281, 95

Postman, M. et al. 1996, AJ, 111, 615

Postman, M. et al. 2005, ApJ, 623, 721

Quilis, V., Moore, B., & Bower, R. 2000, Science, 288, 1617

Quillen et al. 2007, ApJS in press, (astro-ph/0711.1118)

Quintero, A. D., Berlind, A. A., Blanton, M. R., & Hogg, D. W. Submitted to ApJ (astro-ph/0611361)

Richstone, D., 1975, ApJ, 200, 535

Rogers, B., Ferreras, I., Lahav, O., Bernardi, M., Kaviraj, S., & Yi, S. K. 2007, MNRAS, 382, 750

Schawinski, K. et al. (S06) in press, (astro-ph/0601036)

Schlegel, D. J., Finkbeiner, D. P., & Davie, M. 1998, ApJ, 500, 525

Shectman, S. A. 1985, ApJS, 57, 77

Silk, J. 1976, ApJ, 208, 646

Sorrentino, G. & Rifatto, A. 2007, astro-ph/0701460

Stoughton, C. et al. 2002, AJ, 123, 485

Strauss, M. A. et al. 2002, AJ, 124, 1810

Tanaka, M, Goto, T., Okamura, S., Shimasaku, K. & Brinkmann, J. 2004, AJ, 128, 2677

Thomas, D., Maraston, C., & Bender, R. 2005, ApJ, 621, 673

Toomre, A. & Toomre, J. 1972, ApJ, 178, 623

Tully, R. B. 1988, AJ, 96, 73

Valluri, M. 1993, ApJ, 408, 57

van der Marel, R. P., Magorrian, J., Carlberg, R. G., Yee, H. K. C., & Ellingson, E. 2000, AJ, 119, 2038

van Dokkum, P. & Quadri, R. 2007, astro-ph/0704.1760

Visvanathan, N. & Sandage, A. 1977, ApJ, 216, 214

von der Linden, A., Best, P. N., Kauffmann, G., & White, S. D. M. 2007, MNRAS, 379, 867

Weinmann, S. M., van den Bosch, F. C., Yang, X., & Mo, H. J.

White, S. D. M. 1976, MNRAS, 174, 19

Whitmore, B. C. & Gilmore, D. M. 1991, ApJ, 367, 64

York, D. G. et al. 2000, AJ, 120, 1579

Zwicky, F., Herzog, E. Wild, P., Karpowicz, M., & Kowal, C. 1961-1968, Catalog of Galaxies and Clusters of Galaxies, Vol. 1-6, Caltech, Pasadena

국문요약

공간밀도가 은하단내 은하에 미치는 영향

윤주헌

연세대학교 대학원

천문우주학과

은하단은 수많은 은하들이 존재하는 우주에서 밀도가 가장 높은 지역이다. 많은 은하들이 서로에게 영향을 주기 때문에 주변 환경이 은하의 진화에 큰 영향을 미친다. 이러한 주변 환경 효과를 공부하기 위해서는 잘 정리된 은하단의 목록이 필요하다. 최근 성공적으로 진행되고 있는 탐사천문학의 결과, 수많은 은하들의 적색편이를 측정하는 것이 가능해 졌으며 이를 이용하면 균일한 특성을 가진 데이터를 사용한 은하단 연구가 가능하다. 그러나 이러한 탐사연구의 문제점은 적색편이 측정 시 사용되는 광섬유의 한계 때문에 아주 은하의 밀도가 높은 곳에서 모든 은하를 관측하지 못하게 된다는 것이다. 이 연구에서는 은하단내 은하의 색과 등급이 좋은 상관관계를 보인다는 color-magnitude relation을 이용하여 이러한 문제점을 최소화 하였다. 이를 통해 좀 더 실제적인 은하의 밀도측정이 가능해 졌으며 212개의 새로 발견된 것들을 포함하여 총 924개의 은하단을 발견하였다. 이 목록을 이용하여 은하단내 은하들의 색과 등급의 반경에 따른 관계를 연구하였다. 은하들의 색과 등급은 은하반경과 통계적으로 큰 상관관계를 보이지 않았다. 반면에 은하단 중심일수록 만기형 은하들의 비율은 증가하였으며 조기형 은하들의 비율은 감소하였다. 이를 은하의 색으로 봤을 때도 역시 같은 현상을 보였다. 이를 통해 이미 잘 알려진 은하형태-밀도 관계를 확인하였으며 은하단 중심에서 붉은 은하가 많게 보이는 것은 이 은하형태-밀도 관계에 의한 부수적 효과임을 확인하였다. 이러한 은하형태-밀도 관계는 밀도가 높은 은하단일수록 더 뚜렷하게 나타났다. 그리고 일반적인 은하와 다른 특성을

보인다고 알려진 은하단내 가장 밝은 은하인 BCG를 연구하였다. 이 BCG들은 밀도가 증가할수록 그 밝기가 증가하는 반면 그 색은 변하지 않는다는 것이 밝혀졌다. 이 밝기-밀도 관계는 가장 밝은 은하뿐만이 아니라 은하단내 다른 은하들도 비슷한 관계를 보였다. 이점에서 은하단내 은하들은 비슷한 성질을 보인다고 판단된다. 밀도가 낮은 곳에 존재하는 은하들은 BCG를 비롯한 은하단내 은하들에 비해 같은 밝기를 갖더라도 더 푸른색을 띄었으며 통계적인 검증결과 서로 다른 종족임을 보였다. 이를 통해 볼 때 은하단내 은하들의 진화는 밀도가 낮은 곳의 은하들에 비해 다르다고 생각된다.

핵심되는 말 : 목록, 탐사천문, 은하단, 은하진화